Atmos. Chem. Phys. Discuss., doi:10.5194/acp-2017-79, 2017
Manuscript under review for journal Atmos. Chem. Phys.
Discussion started: 30 March 2017

Atmospheric Chemistry and Physics Discussions

Atmospheric pollution concentrations over the Eastern Mediterranean during summer – A review

Uri Dayan[1], Philippe Ricaud[2], Régina Zbinden[2] and François Dulac[3]

[1]Department of Geography, The Hebrew University of Jerusalem, Jerusalem, 91905, Israel

[2]CNRM, Météo-France, CNRS UMR3589, Toulouse, France

[3]Laboratoire des Sciences du Climat et de l'Environnement (IPSL-LSCE), CEA-CNRS-UVSQ, Univ. Paris-Saclay, Gif-sur-Yvette, France

Correspondence to: Uri Dayan (msudayan@mscc.huji.ac.il)

Abstract. The Eastern Mediterranean (EM) is one of the regions in the world where elevated concentrations of primary and secondary gaseous air pollutants have been reported frequently, mainly in summer. This review discusses published studies of the atmospheric dispersion and transport conditions characterizing this region during the summer, followed by a description of some essential studies dealing with the corresponding concentrations of air pollutants such as ozone, carbon monoxide, total reactive nitrogen, methane and sulfate aerosols observed there.

The interlaced relationship between the downward motion of the subsiding air aloft induced by global circulation systems affecting the EM and the depth of the Persian Trough, a low-pressure trough that extends from the Asian monsoon at the surface controlling the spatio-temporal distribution of the mixed boundary layer during summer is discussed. The strength of the wind flow within the mixed layer and its depth affect much the amount of pollutants transported and determine the potential of the atmosphere to disperse contaminants off their origins in the EM. The reduced mixed layer and the accompanying weak westerlies, characterizing the summer in this region, lead to reduced ventilation rates, preventing an effective dilution of the contaminants. Several studies pointing at specific local (e.g. ventilation rates) and regional peculiarities (long-range transport) enhancing the building up of pollutant concentrations are presented.

Atmos. Chem. Phys. Discuss., doi:10.5194/acp-2017-79, 2017
Manuscript under review for journal Atmos. Chem. Phys.
Discussion started: 30 March 2017

Atmospheric Chemistry and Physics Discussions

Tropospheric ozone concentrations observed in the summer over the EM are among the highest over the Northern Hemisphere. The three essential processes controlling its formation (i.e., long-range transport of polluted air masses, dynamic subsidence at mid-tropospheric levels, and stratosphere-to-troposphere exchange) are reviewed. Airborne campaigns and satellite-borne initiatives have indicated that the concentration values of reactive nitrogen identified as precursors in the formation of ozone over the EM were found to be 2 to 10 times higher than in the hemispheric background troposphere. Several factors favor sulfate particulate abundance over the EM. Models, aircraft measurements, and satellite derived data, have clearly shown that sulfate has a maximum during spring and summer over the EM. The carbon monoxide (CO) seasonal cycle, as obtained from global background monitoring sites in the EM is mostly controlled by the tropospheric concentration of the hydroxyl radical (OH), and therefore demonstrates high concentrations over winter months and the lowest during summer when photochemistry is active. Modeling studies have shown that the diurnal variations in CO concentration during the summer result from long-range CO transport from European anthropogenic sources, contributing 60 to 80% of the boundary-layer CO over the EM. The values retrieved from satellite data enable us to derive the spatial distribution of methane (CH_4), identifying August as the month with the highest levels over the EM. The outcomes of a recent extensive examination of the distribution of methane over the tropospheric Mediterranean Basin, as part of the Chemical and Aerosol Mediterranean Experiment (ChArMEx) program, using model simulations and satellite measurements is coherent with other previous studies. Moreover, this methane study provides some insights on the role of the Asian monsoon anticyclone in controlling the variability of CH_4 pollutant within mid-to-upper tropospheric levels above the EM in summer.

1 Introduction

The relationship between atmospheric pollutant concentrations and large-scale atmospheric circulation systems have been examined over the past decades (e.g., Davis and Kalkstein, 1990; Dayan et al., 2008). This strong relationship and its issuing dispersion condition at several scales, and climatically related variables such as air pollutants, is presented in this work as part of the Chemistry-Aerosol Mediterranean Experiment (ChArMEx; http://charmex.lsce.ipsl.fr).

However, a first major drawback in attributing pollutant concentrations to variations in large-scale atmospheric circulation arises from the fact that changes in removal processes and upwind emissions are not necessarily concurrent with variations in circulation. Some efforts were undertaken, mainly through coupled climate-chemistry models to treat and analyze at the same time, the changes in general circulation and atmospheric chemistry (Hein et al., 2001; Dastoor and Larocque, 2004). Moreover, secondary pollutants such as tropospheric ozone result basically from photochemical reactions among precursors and as such, are controlled by air mass characteristics such as temperature and humidity, and cloud cover/solar radiation. Accordingly, changes in trace gases concentrations are modified by exposure to differing air masses as governed by changes in atmospheric circulation.

A second substantial shortcoming in trying to associate changes in pollutant concentration to variation in circulation patterns is their different life span and distribution. For example, durable greenhouse gases (GHG) such as methane (CH_4) and carbon dioxide (CO_2) as compared to aerosols which are most relevant for short spatial and temporal scales (Andreae, 2001; Voulgarakis et al., 2010). Radiative forcing of aerosols is of much higher spatial variability than GHG forcings due to the relatively short aerosol lifetime (daily-weekly scale) compared to that of GHG (monthly-yearly scale).

Lelieveld et al. (2002) studied air pollutant transport over the EM in summer time. They report that the synoptic flow is controlled by the strong east-west pressure difference between the Azores high and the Asian monsoon low, with additional influence in the upper troposphere from the Tibetan anticyclone. This yields a contrasted situation in the tropospheric column with European influence in the lowermost troposphere, a much longer-range transport from Asia and North America at mid-tropospheric levels, and a major impact from Asia in the upper troposphere and lower stratosphere.

In this review, centered over the Eastern Mediterranean (EM) during the summer season, we first describe the atmospheric dynamic conditions favoring the building up of tropospheric pollutant concentrations. Secondly, we propose a synthesis of the essential studies on air pollutant concentrations including ozone (O_3), sulfate aerosols (SO_4), total reactive nitrogen (NOy), carbon monoxide (CO), and methane (CH_4). The sources of the data reported include in-situ observations,

balloon-sounding, aircraft and space-borne observations as well as model data which results, in terms of dynamics, are mostly updated over 1948-2016 on availability.

2 Summer atmospheric dynamic conditions favoring the building up of tropospheric pollutants concentrations

Different spatial and temporal scales of motion affect pollutant transport and dispersion: the microscale, mesoscale, synoptic scale, and macro-, or global scale. At the scale of a few months, the planetary boundary layer is relatively well mixed. However, on shorter timescales and near the Earth's surface (where pollutants are emitted), transport and dispersion are often limited by atmospheric conditions. In this section, we will focus on the global and synoptic scale processes that favor a potential accumulation of pollutants in the EM troposphere.

2.1 Global and synoptic scales inducing subsiding conditions over the Eastern Mediterranean

In general, the atmospheric conditions over the EM are persistent during the summer and subject to two essential processes. The first is the cool advection at shallow tropospheric layers caused by the strong, dry north Etesian winds generated by the Persian Trough (PT). This surface low pressure trough extends from the Asian monsoon through the Persian Gulf and further, along southern Turkey to the Aegean Sea (Figs. 1 and 2). The second is the dynamic subsidence generated by several global-scale processes: the African Monsoon as part of the subtropical descending branch of the Hadley cell (Fig. 3 left), the Asian Monsoon as part of the Walker cell (Fig. 3 right) and subsidence caused by the negative relative vorticity characterizing this region, during summer, as explained further on.

However, subsidence is neither restricted to mid-tropospheric levels nor solely associated to the descending branch of these both general circulation cells. In summer, at higher atmospheric layers, air masses converge and subside over the EM as contributed by both an anticyclonic curvature caused by the eastward progression of the Subtropical high, and an anticyclonic wind shear as related to the position of the Subtropical Jet. Under these circumstances the southeastern part of the EM is exposed to the southern flank of the jet and therefore prone to negative shear vorticity. Although shear vorticity is an order of magnitude smaller than planetary vorticity, nearby jet streak

makes this relative vorticity component significant due to the strong change in wind speeds across the jet. Contribution of both components enhances negative vorticity resulting in a total long- term mean negative vorticity of -1 to -3 10^{-5} s^{-1} at 200 hPa (~12 km above sea level; a.s.l.) featuring the summer season over the EM (Fig. 4).

The contribution of the above-mentioned dynamic subsidence generated by all processes results in positive Omega values, defined as the Lagrangian rate of change in pressure with time, indicating a downward air motion over the whole EM with its highest core of maximum subsidence over Crete as depicted over mid-tropospheric levels (500 hPa geopotential height) (Fig. 5).

Following the subsidence caused by the large-scale downward motion, the warming and drying up is manifested by the delimiting sharp decrease in relative humidity over the EM Basin (Fig. 6).

Based on National Centers for Environmental Prediction/National Center for Atmospheric Research (NCEP/NCAR) reanalysis for 2000–2012, Lensky and Dayan (2015) have recently shown that the coincidence of negative vorticity advection aloft accompanied by cold horizontal advection, at lower tropospheric levels, featuring the EM during PT synoptic conditions drives the wind flow out of the thermal wind balance inducing a vertical downward motion (Figs. 2 and 7).

Rodwell and Hoskins (1996) used an idealized model to explain the strong descent on the subtropics attributed to the African Monsoon Hadley cell, and suggested that the monsoon-forced adiabatic descent may result in clear air and, therefore, a local diabatic enhancement which effectively doubles the strength of descent. Ziv et al. (2004) found that the cool advection associated to the PT (Fig. 2) and the subsidence related to both descending branches of the African and Asian Monsoons (Fig. 3) are interrelated and tend to balance each other. They suggest that this compensation mechanism explains the reduced day to day temperature variations over the eastern part of the basin in summer (Fig. 8).

However, this monotonic regime is interrupted by the occurrence of hot day events resulting from an expansion of the Subtropical High from North Africa towards the EM which are prone for elevated concentration of air pollutants. Harpaz et al. (2014) found that such episodes are confined to the lower 4 km and controlled by the intensity of the negative temperature advection rather than by the prevailing subsidence.

Atmos. Chem. Phys. Discuss., doi:10.5194/acp-2017-79, 2017
Manuscript under review for journal Atmos. Chem. Phys.
Discussion started: 30 March 2017

Atmospheric Chemistry and Physics Discussions

2.2 Atmospheric mixing layer depth over the Eastern Mediterranean coastal zone

The vertical velocity involved in the mixing process within the turbulent layer near the surface and specifically its depth are important parameters in determining air pollutant concentrations at shallow tropospheric levels (Zhang and Rao, 1999). The changes in the mixing layer depth (MLD, i.e. the height of the convective atmospheric boundary layer marked by the base of a thermal inversion) is governed by several factors: surface heating (Holtslag and Van Ulden, 1983), horizontal advection determined by the intensity of the sea breeze in coastal areas (McElroy and Smith, 1991; Lensky and Dayan, 2012), local terrain over the continent (Kalthoff et al., 1998), and the strength of the subsiding atmospheric air mass capping the mixed layer, defined by the temperature profile within this stable layer and synoptic scale vertical motion (Dayan et al., 1988). Since this turbulent layer is mainly governed by synoptic-scale circulation patterns, both the surface synoptic systems and their associated upper tropospheric conditions should be taken into consideration for understanding the behavior of the MLD over the EM basin and its adjacent coastal region.

Within the EM, most of the studies on the relationship between synoptic circulation and the structure of the MLD over the continental EM were conducted in Israel, the southeastern part of the basin. In particular, several studies were undertaken to characterize the spatial and temporal behavior of the MLD (Neumann, 1952; Halevy and Steinberger, 1974; Rindsberger, 1974, 1976; Dayan et al., 1988; Glaser et al., 1993; Lieman and Alpert, 1993; Dayan et al., 1996; Dayan and Rodnizki, 1999; Dayan et al., 2002; Ziv et al., 2004) using sounding measurements at the Israel Meteorological Service permanent site in Beit-Dagan (31.99°N, 34.82°E, 39 m a.s.l.), 8 km southeast of Tel Aviv and at other sporadic sounding sites.

The atmospheric noon-time mixed layer during the summer over the EM region is featured by a persistent elevated inversion base formed by a clear boundary line separating two differing air masses, a cool and humid mass above ground capped by a much warmer and subsiding dry air. The MLD is controlled by the interlaced relationship between the downward motion of the subsiding air aloft and the depth of the PT at the surface (Fig. 9).

Due to the existing correlation between the MLD featuring the PT and air pollution episodes over the EM evidenced in previous studies (Dayan and Graber 1981; Dayan et al., 1988; Koch and

Dayan, 1992), this barometric system was classified into three essential types (Fig. 10) defined by the surface-pressure difference between Nicosia (35.16°N, 33.36°E, 149 m a.s.l.) in Cyprus and Cairo (30.1°N, 31.4°E, 75 m a.s.l.) in Egypt, and the temperature at 850-hPa in Beit-Dagan (Israel):

a) Moderate PT: with a horizontal pressure, gradient Nicosia-Cairo within 1.0–1.9 hPa, or even greater than 1.9 hPa in case the 850 hPa temperature exceeds 20°C; this surface pressure pattern occurs usually in tandem with a weak zonal flow aloft, on the northern edge of the subtropical high pressure system;

b) Shallow PT: with a horizontal pressure gradient (Nicosia–Cairo) less than 0.9 hPa topped by an upper atmospheric ridge;

c) Deep PT: deepening of the PT described in b), due to a temporary retreat of the subtropical high, featured by a cyclonic flow aloft; there, the pressure gradient (Nicosia–Cairo) exceeds 2.0 hPa and the 850-hPa temperature is less than 20°C.

Analyses of upper air measurements carried out regularly at Beit-Dagan, in the central coastal plain of Israel, point at significant differences of the MLD for the several modes of the PT. The overall summer mean noon time mixing depth values for 1981-84 is 764 ±320 m (Dayan et al., 1988). A classification along the modes defined above resulted in mean and standard deviation values of 428 ±144 m and 1010 ±214 m for the shallow and deep mode respectively (Koch and Dayan, 1992). The spatial distribution of the mixing depth is rather homogeneous under deep PT conditions over the central coastal plain of Israel as compared to the shallow mode where its value is kept almost uniform above sea-level while penetrating inland. However, the thickness of the mixed layer changes markedly, for the first kilometers, when moving onshore from the coastline inland. The parabolic profile for inland MLD variation, suggested on theoretical grounds (Stunder and Sethuraman, 1985) and observed empirically by Berman et al. (1999) indicates that interior land sites tend to develop the highest average daytime MLD with values falling rapidly as the coastline is approached and reaching minimum values less than 500 m offshore.

Due to the important implication of this behavior on the building up concentration of air pollutants, the lateral variance of the mixing depth was tested for part of the upper air measurements performed at 4 sites concurrently during the 1981-1984 campaign (Dayan et al., 1988). These sites

on a west-east transect were: Nizanim (31.7°N, 34.63°E, 10 m a.s.l.) on the southern coastal shore of Israel; Beit-Dagan (31.99°N, 34.82°E, 39 m a.s.l.) on the coastal plain; Ruchama (31.5°N, 34.7°E, 210 m a.s.l.) ~20 km inland in the northern Negev Desert; and Jerusalem (31.77°N, 35.21°E, 786 m a.s.l.). The average thickness of the mixed layer when moving from the coast inland is reduced by 350 m while reaching Jerusalem (Fig. 11). This result is consistent with Halevy and Steinberger (1974). However, airplane measurements indicate that the top of the mixed layer over the Dead Sea, located ~80 km inland, is within 1400–1600 m a.s.l.

This marked onshore decrease in the MLD has an important implication by influencing the pollution transported from the EM inland (Luria et al., 1984; Alper-Siman Tov et al., 1997; Luria et al., 1996). Dayan et al. (1988) has tested the longitudinal variance of the MLD North-South vertical cross section on 21 summer noon-time upper air measurements performed simultaneously at 3 sites ~60 km apart along the Israeli coast: Beit-Dagan, Ruchama and Revivim (31.04° N, 34.72° E, 286 m a.s.l.). Their respective MLD mean was evaluated to 896, 781 and 805 m a.s.l. with a standard deviation of 439, 401 and 329 m a.s.l., respectively.

A comparison between these 3 MLDs revealed that the mixed layer at Beit-Dagan is significantly thicker than either at Ruchama or Revivim. This finding is explained by the greater distance of the southern sites (i.e., Ruchama and Revivim) from the cyclonic core of the PT (which persists in summer to the northeast of Israel) as well as the decreased distance from the anticyclonic center of the North African subtropical high (which persists during all seasons to the southwest of Israel). The lateral and longitudinal spatial MLD above-mentioned values indicate that the most reduced summer MLDs are expected over the southeastern coast of the EM.

Characterizing the structure of the MLD spatial variation offshore over the EM basin is of importance for getting a better insight on the processes which control the dispersion of contaminants over the sea. Few investigators (Gamo et al. (1982) and Kuwagata et al. (1990) for Japan; Stunder and Sethuraman (1985) for the United States; Gryning (1985) for Denmark) have analyzed the spatial variations of the atmospheric mixing layer in coastal areas. Similar studies as related to the EM Basin are quite limited and deal also mainly on the conditions not directly located over the open sea but rather at sites distant from the coast line.

In a 2006-2011 study based on a remote sensing tool, the European Center for Medium Range Weather Forecasts (ECMWF) (model and radiosonde observations launched at Thessaloniki's airport (Greece, 40.6°N, 22.9°E, 10 m a.s.l.) ~1km from the coastline, Leventidu et al. (2013) found the MLD seasonal cycles peak with a summer maximum of 1400, 1800, and 2100 m a.s.l. in June, July and August, respectively. In the unique study of this type we are aware of, Dayan et al. (1996) have evaluated the spatial and seasonal distribution of the MLD over the whole Mediterranean Basin. Based on ~65000 air measurements from 45 radiosonde stations within and surrounding the basin from spring 1986 through winter 1988, the MLD was derived from the potential temperature gradient measured within the boundary layer and the capping stable layer above it. As expected, the summer values prove to be generally higher over land and minimum over the most eastern and western limits of the Mediterranean Basin (Fig. 12). They concluded that the distance from the coastline and topography are the main factors influencing the spatial distribution of the MLD. The steep gradient in MLD values observed as moving onshore is consistent with the elevated summer values in Thessaloniki (Greece) reported by Leventidu et al. (2013).

Moreover, Dayan et al. (1996) found that the most striking temporal effect on MLD distribution over the basin is caused by synoptic weather systems and the intensity of the sea-breeze along the coast. The diminishing of the MLD over the Mediterranean Basin as moving from its center eastwards toward the EM coast they have observed is consistent with the unique series of measurements of the temperature profiles performed during the summer of 1987 near Ashdod Harbor (31.82°N, 34.65°E), some 40 km south of Tel-Aviv (Israel) at 2 to 22 km from shore using a tethered balloon where prominent inversion bases of 350 to 600 m a.s.l. were observed (Barkan and Feliks, 1993). Moreover, such limited MLD values over the sea were obtained in the airborne Gradient in Longitude of Atmospheric constituents above the Mediterranean basin (GLAM) campaign in August 2014 (Zbinden et al., 2016): the MLD over the sea measured in the period 6-10 August 2014 was approx. 800 m a.s.l. over Crete diminishing to about 400–500 m a.s.l. over Cyprus.

2.3 Diurnal behavior of the mixing layer depth over the Eastern Mediterranean coastal zone

The diurnal behavior of the mixed-layer depth is assessed in the coastal plain of the EM based on routine radiosonde ascents that are, unfortunately, of coarse temporal resolution. The MLD reaches

a summer minimum at 750 m and a winter maximum at1800 m. The hourly maximum MLD is between 23:00 UTC and 05:00 UTC for all seasons and decreases gradually toward its minimal value at 18:00 UTC.

However, since this cycle is governed mainly by synoptic weather systems, and the strength of the sea-breeze, this behavior would be more significant for the summer. During this season, the variation of the mixed-layer height due to diurnal variations of solar radiation and local terrain effects is not obstructed by large-scale variations caused by frequent transitions between different synoptic configurations, as featured by other seasons. Consequently, MLD variation is most evident during the summer, mainly controlled by the daily sea-breeze cycle and heat fluxes that are most intensive then. The layer minimal depth, along the coast, is usually observed during late afternoon hours when heat fluxes dissipate rapidly and the wind speed of the cool sea breeze reaches its minimal rate. This process results in a decrease of the marine turbulent boundary layer (Dayan and Rodnizki, 1999).

In series of measurements in June and August 1987 conducted over the sea near the Israeli coast, Barkan and Feliks (1993) found a prominent diurnal oscillation in the inversion base. During daytime, the inversion base moved downward reaching its minimum height (250–450 m a.s.l.) in the afternoon and evening. During the night, it moved upward reaching its maximum height in the late night and early morning (450–850 m a.s.l.). These diurnal variations are due to the intensity of the sea and land breezes as shown by Feliks (1992).

2.4 Ventilation rates over the Eastern Mediterranean coastal zone

The rate of potential transport of atmospheric pollutants is strongly affected by the strength of the wind flow within the mixed layer and by its depth. Further along the EM coastal zone, both coastal-breeze circulation and large-scale synoptic situation regulate the mean MLD. Assessing the atmospheric dispersion conditions is commonly derived from the ventilation rates calculation. This term is the MLD multiplied by the mean wind speed in the mixed layer, representing the potential of the atmosphere to dilute and transport contaminants away from a source region. Matvev et al. (2002) have calculated over 1948-1999 the mean and standard deviation of the mixing depth, wind speed and long-term range of ventilation rates at the Israel Meteorological Service sounding site

Atmos. Chem. Phys. Discuss., doi:10.5194/acp-2017-79, 2017
Manuscript under review for journal Atmos. Chem. Phys.
Discussion started: 30 March 2017

in Beit-Dagan (Israel). Their results in Table 1 clearly show that the reduced ventilation rates characterizing the EM during summer inhibit an efficient dispersion of pollutants.

Table 1: Monthly long-term means (LTM) and standard deviation (S.D.) of the mixing layer depth (MLD), wind speed and range of ventilation rates over Beit-Dagan in the central coast of the EM. LTM and S.D. values for MLD for the years: 1955-1968 (Rindsberger 1974), 1981-1984 (Dayan et al. 1988), 1987-1989 (Dayan and Rodniski 1999). LTM and S.D. values for wind speeds are from the NCEP/NCAR Reanalysis Project (NOAA- CIRES Climate Diagnostic Center) for a 51-year data record: 1948-1999 from their Web site at http://www.esrl.noaa.gov/psd/ (from Matvev et al. (2002), permission requested from Elsevier).

	MLD		Wind Speed		Ventilation Rates
Month	LTM (m)	S.D. (m)	LTM (m s^{-1})	S.D. (m s^{-1})	Range of LTM (m^2 s^{-1})
January	1700	950	7.0	4.75	1688 – 31138
February	1830	1135	7.5	5.00	1738 – 37063
March	1790	860	7.0	4.75	2093 – 31138
April	850	660	5.5	3.75	333 – 13968
May	750	525	4.5	3.25	280 – 9880
June	810	470	5.5	2.25	1105 – 9920
July	870	450	5.0	1.65	1365 – 8780
August	820	395	4.5	1.50	1275 – 7290
September	930	510	5.0	2.10	1218 – 10224
October	1650	910	4.5	3.50	740 – 20480

Atmos. Chem. Phys. Discuss., doi:10.5194/acp-2017-79, 2017
Manuscript under review for journal Atmos. Chem. Phys.
Discussion started: 30 March 2017

November	1500	940	5.5	4.50	560 – 24400
December	1700	990	6.0	4.50	1065 – 28245

2.5 Air mass origins over the Eastern Mediterranean

Studies of the long-range transport (LRT) of pollution by trajectory models help us interpret and better define the movement and removal processes affecting atmospheric concentrations. Although changes in wind direction are observed on a diurnal and seasonal basis depending on the synoptic conditions affecting the region, the prevailing wind flows over the EM are from the west towards the east. Therefore, air pollutants emitted from upwind sources to the west of the EM will reach the EM and will be added to those emitted locally. Indeed, numerous observational and modeling studies have confirmed that the EM is affected by the long-range transport of air pollutants originating from Europe (e.g., Dayan, 1986; Luria et al., 1996; Wanger et al., 2000; Erel et al., 2002, 2007 and 2013, Matvev et al., 2002; Rudich et al., 2008; Drori et al., 2012).

To get an insight on the LRT over the EM, the Air Resources Laboratory's trajectory model (GAMBIT- Gridded Atmospheric Multi-Level Backward Isobaric Trajectories; Harris, 1982) was applied over 1978-1982 (Dayan, 1986). The duration of each trajectory was chosen as 5-days backward in time enabling the tracing of air masses originating from Europe, the Mediterranean Basin (MB), North Africa and the Near East close to the EM central coast of Israel (Fig. 13).

The input wind data for GAMBIT, which originate at the National Meteorological Center (NMC) in Suitland, Maryland (USA), consist of gridded wind components at standard pressure levels produced by a global atmospheric model. The GAMBIT calculates trajectories to each receptor twice daily at standard pressure surfaces. The 850-hPa level (~1500 m a.s.l.) was chosen as the most representative of the transport layer. This level is selected as the intermediary level between the surface wind regime and the regime of upper winds relatively free from local surface effects. Trajectory direction was divided into five distinctive geographical classes as shown in Figure 13. Respective occurrences and seasonal distributions can be summarized as follows:

1) Long fetch of maritime air masses from northwest Europe crossing the Mediterranean Sea, accounting for 36%, was the most frequent on average and fell evenly throughout the whole year;

2) Northeast continental flow that originated in Eastern Europe, accounting for 30%, was the most frequent during the summer season;

3) Southeast flow from the Arabian Peninsula, accounting for 5%, was infrequent, occurring mainly during the autumn;

4a) Southwest flow along the North African coast, accounting for 11%, was the most frequent during late winter and spring; and

4b) South-southwest flow from inland North Africa was accounting for 7%, with a late winter and spring maximum.

Therefore, 1) and 2) trajectory types are indeed predominant with a summer maximum occurrence (>66%) over the EM.

3. Summer atmospheric pollutant concentrations

The EM is one of the regions in the world where elevated concentration of primary and secondary gaseous air pollutants has been reported frequently. This region is influenced not only by local atmospheric dispersion conditions but also by the ability of the atmosphere to inherit a significant proportion of pollutants from European sources and mineral dust that arrive from two major source regions: the North African Sahara and the Arabian deserts. However, in general, mineral dust does not affect the EM during summer (e.g., Dayan et al., 1991; Moulin et al., 1998; Sciare et al., 2003) and they are not in the scope of this study focused on summer conditions.

After reviewing the atmospheric dispersion and transport conditions characterizing the EM during the summer, a summary of the essential results published over the last decade dealing with trace gases and anthropogenic sulfate aerosol concentrations over this region is presented. These studies demonstrate how the above described global and synoptic scale processes control the extent of trans-boundary transport of air pollutants and chemical composition and concentrations over the EM.

3.1 Processes controlling O_3 formation

Most tropospheric O_3 formation occurs when nitrogen oxides (NOx), carbon monoxide (CO) and volatile organic compounds (VOCs) react in the atmosphere in the presence of sunlight. Due to cloud free conditions, high incoming solar radiation characterizes the EM during summer (Lelieveld et al., 2002) which enhances the building-up of O_3 concentrations.

Numerous researchers have identified the EM as a hot spot" of summertime tropospheric ozone (e.g., Stohl et al., 2001; Roelofs et al., 2003; Zbinden et al., 2013; Zanis et al., 2014; Doche et al., 2014; Safieddine et al., 2014).

Zbinden et al. (2013) derived the climatological profiles and column contents of tropospheric O_3 from the Measurements of Ozone by Airbus Aircraft program (MOZAIC) over the mid-northern latitudes (24°N to 50°N) over the 1994-2009 period. Among the 11 most visited sites by the MOZAIC aircrafts, is the EM cluster which comprises 702 profile data from Cairo (31.39°E, 30.10°N) Egypt and Tel-Aviv (34.89°E, 32.00°N) Israel airports from which monthly means were derived. The O_3 volume mixing ratio obtained were converted to Dobson units (DU) and validated against coincident ozonesonde profiles. Considering all sites, the EM reaches the largest tropospheric O_3 column concentration of 43.2 DU in July, in agreement with the summer extreme found by Ziemke et al. (2011), pointing at the favorable photochemical conditions characterizing this region.

Zanis et al. (2014) identified a summertime pool with high O_3 concentrations in the mid-troposphere over the EM over the 1998-2009 period as derived from the ERA-Interim reanalysis O_3 data, Tropospheric Emission Spectrometer (TES) satellite O_3 data, and simulations with the EMAC (ECHAM5–MESSy) atmospheric chemistry–climate model. They indicated that the high O_3 pool over the mid-troposphere is controlled by the downward transport from the upper-troposphere and lower-stratosphere over this part of the MB, which is characterized by large-scale subsidence. This subsidence is regulated by the Asian Monsoon as described in Section 2.1. Furthermore, Zanis et al. (2014) based on previous case studies (e.g., Galani et al., 2003; Akritidis et al., 2010) and climatological studies (e.g., Sprenger and Wernli, 2003; James et al., 2003) and their own results deduced that the mechanism leading to high tropospheric O_3 over the EM consists of two essential consecutive phases. Enrichment of stratospheric O_3 into the upper-troposphere via a stratosphere-to-troposphere transport process. In the second stage, these ozone-rich air masses are transported downward by the strong summertime subsidence characterizing this region.

Atmos. Chem. Phys. Discuss., doi:10.5194/acp-2017-79, 2017
Manuscript under review for journal Atmos. Chem. Phys.
Discussion started: 30 March 2017

Doche et al. (2014) analyzed tropospheric O_3 concentrations for the 2007-2012 period as observed over the MB by the Infrared Atmospheric Sounding Interferometer (IASI). They identified an abrupt west–east O_3 gradient in the lower troposphere over the MB with the highest concentrations observed over its eastern part. These concentrations were observed at mid-tropospheric layers (3 km) caused by subsiding ozone-rich air masses from the upper-troposphere, typifying summer. A clear and consistent seasonal variability emerges from their measurements, showing a maximum of the 3-km partial column O_3 concentration in July (Fig. 14). This is consistent with the study of Tyrlis and Lelieveld (2013) who found that the key global and synoptic driving factors yielding to high O_3 concentrations in July is the strength of the Etesian winds and the subsidence over the EM, which is temporally very well correlated with the Indian monsoon.

Based on IASI measurements and the Weather Research and Forecasting Model with Chemistry (WRF-Chem), Safieddine et al. (2014) have shown that the air column of the first 2 km above ground is enriched by anthropogenic O_3. Above 4 km, O_3 is mostly originating from outside the MB by LRT process or generated through stratosphere-to-troposphere exchange characterizing the eastern part of the MB during the summer.

Air masses from surrounding regions in the EM atmosphere have a great impact on surface O_3 concentrations. In a recent study, Myriokefalitakis et al (2016) have investigated the contribution of LRT on O_3 and CO budget in the EM basin, using a global chemistry transport model (CTM), the TM4-ECPL, driven by ECMWF Interim re-analysis project (ERA-Interim) meteorology (Daskalakis et al., 2015). They found that about 8% of surface O_3 concentrations are affected by local anthropogenic emissions, whereas subsiding air masses from the free-troposphere and horizontal transport from surrounding regions provide about 38% and 51% of O_3 sources, respectively, into the EM-MLD. Although elevated O_3 concentrations over the EM during the summer are mainly attributed to LRT of polluted air masses originating from Europe and lingering over the MB, its enhancement as a secondary pollutant is also caused by its precursors emitted along the coasts of the EM. Consequently, several studies dealing with O_3 concentrations measured over coastal sites surrounding the EM and its inland penetration are presented.

O_3 measurements were performed over the northern coast of Crete, at Finokalia (35°30′N, 25°70′E) 70 km northeast of Heraklion, from September 1997 to September 2000 and from a rural area (40°32′N, 23°50′E) close to Thessaloniki in the north of Greece from March 2000 to January 2001.

Based on these measurements, Kouvarakis et al. (2002) pointed out the existence of a well-defined seasonal cycle in boundary layer O_3, with a summer maximum both above the Aegean Sea and at Finokalia. They indicated that LRT is the main factor accounting for the elevated O_3 levels above the EM. This finding is consistent with the 1997–2004 surface O_3 time series at Finokalia (Crete) of Gerasopoulos et al. (2005) who investigated the mechanisms that control O_3 levels and its variability. They identified transport from the European continent as the main mechanism controlling the O_3 levels in the EM, especially during summer when O_3 reaches a July maximum of 58 ±10 ppbv. Moreover, on a larger regional scale, Kourtidis et al. (2002) used ozonesonde ascents, lidar observations, ship cruises, and aircraft flights, to show that south and southwestern synoptic flows associated with Saharan dust events result in lower O_3 above the planetary boundary layer by 20–35 ppbv as compared to these during northerly flows, which transport air from continental Europe. Kleanthous et al. (2014) based on sixteen years of O_3 concentrations measured at the EMEP Agia Marina Xyliatou rural station (Cyprus) and 3 other remote marine sites, over the western, central and eastern parts of the island have shown that local precursors contribute to only about 6% (~3 ppbv) of the observed O_3. However, elevated concentrations of this secondary pollutant occurring in summer are attributed to LRT of air masses mainly originating from northerly and westerly directions. The summer average annual maximum of 54.3 ±4.7 ppb was observed to be related to the transport of polluted air masses from Near-Asia, East and Central Europe toward Cyprus.

Despite the prevailing synoptic meteorological conditions featuring the EM in summer, the differing pathways of the LRT of polluted air masses can affect differently the buildup of pollutants concentrations. To investigate such changes, Wanger et al. (2000) performed a comprehensive study that included 150 hours of instrumented aircraft monitoring flights comparing two events of air mass transport (September 1993 and June 1994) representing two distinct types of LRT. This airborne study comprised flight paths taken approximately 70 km offshore paralleled to the Israeli coastline and 180 km in length with Tel-Aviv in the center.

These flights were performed during midday under westerly wind flow conditions and at an altitude of 300 m a.s.l. (well within the mixed layer). While both wind flow conditions were nearly similar through the measurement periods and along the 180-km flight path, the air mass sampled in September 1993 was much “cleaner” than the one sampled in June 1994. The O_3 concentration

averaged for the first campaign was 39 ±7 ppb, against 48 ±9 ppb in the second period. Therefore, Wanger et al. (2000) suggested the two air masses travelled different paths before reaching the EM region. Model simulation showed that the pollution sources in southern Europe and the Balkans did not affect the EM coasts in September 1993, contrarily to the synoptic conditions and simulation results for the June 1994 period where the winds over the EM tended to be northwesterly and thus forcing the polluted air masses toward the coasts of the EM.

The summer synoptic and dynamic conditions prevailing over the EM supply the essential ingredients for the building up of O_3 concentrations. Based on the similar climatic conditions between the Los Angeles Basin and the EM, Dayan and Koch (1996) proposed a theoretical description of the cyclic mechanism in summer, leading to fumigation (i.e., a downward dispersion of an enriched O_3 cloud toward the ground) further inland from the EM coast. Under the deep mode of the PT, stronger westerly winds, acting as a weak cold front (Fig. 15, panel A1) penetrate far inland, undercutting the mixed layer polluted by O_3 from the previous day (Fig. 15, panel A2). In this way, part of the mixed layer containing O_3 is pushed upward and isolated from the ground. If the pressure gradient weakens on the following day, the western flow weakens (Fig. 15, panel B1). The cooling effect of the cool and moist marine air is consequently reduced and the convective boundary layer inflates rapidly. When the top of the mixed layer reaches the elevated O_3 cloud, the latter is penetrated by convective currents (Fig. 15, panel B2) and parts of the cloud are entrained toward the ground in this fumigating process.

Elevated O_3 concentrations (>117 ppb) were measured at inland rural sites during the 1988-1991 early summer months (Peleg et al., 1994). Based on air mass back-trajectory analyses, these elevated O_3 mixing ratios at rural sites over central Israel were found only in case of air masses overpassing Tel Aviv metropolitan area. Furthermore, the very low ratio of SO_2/NO_x clearly indicates that O_3 precursors such as nitrogen oxides (NOx, the sum of NO and NO_2), carbon monoxide (CO), and volatile organic compounds (VOC) originate mainly from fossil-fuel combustion from mobile sources (Nirel and Dayan, 2001). These pollutants are subjected to chemical and photochemical transformations in the presence of solar radiation and atmospheric free radicals to form O_3.

Over central Israel, the main source for these precursors emitted along the Israeli coastline is transportation (Peleg et al., 1994). Since O_3 formation and other secondary pollutants takes several

hours, significant transport and mixing occur simultaneously with the chemical reactions (Seinfeld, 1989; Kley, 1997). Thus, increasing urban and commercial activity along the highly populated Israeli coastal region, together with expanding transportation activity in the Gaza region, was found to strongly deteriorate inland air quality and, specifically, to cause increasingly elevated inland O_3 levels. Model results showed that traffic emissions during the morning rush hour from the Tel Aviv metropolitan area contribute about 60% to the observed O_3 concentrations (Ranmar et al., 2002). Moreover, their study showed the summer season features a shallow mixed layer and weak zonal flow, leading to poor ventilation rates which restrict O_3 dispersion efficiency. These poor ventilation rates result in the slow transport of O_3 precursors, enabling their photochemical transformation under intense solar radiation during their travel from the EM coast inland.

However, elevated O_3 concentrations are not limited to the summer over the EM. Dayan and Levy (2002) found 103 ‘‘high-ozone days’’ where O_3 is >80 ppbv for at least 2 hours based on 24 Israeli sites over 1997-1999. From their O_3 temporal analyses they concluded that the highest values are more frequent during the transitional (spring and autumn) seasons (65% of 103 days) than during the summer season (35%).

Based on the recent remote sensing tools in conjunction with meteorological observations and models, we conclude on the three essential processes that control the O_3 concentration during summer at various tropospheric levels over the EM: 1/ in the shallow troposphere, the horizontal transport of O_3-enriched air masses from eastern continental Europe to the region controlled by the position and strength of the Azores High and the PT; 2/ the dynamic subsidence at mid-tropospheric levels; and 3/ the stratosphere-to-troposphere exchange in the upper troposphere. At the surface of the EM coast, during transitional seasons, high O_3 episodes are associated with hot and dry air masses originating east of Israel, where O_3 precursor emissions are negligible, demonstrating that high O_3 levels are more dependent on air mass characteristics than on upwind precursor emissions.

3.2 Particulate sulfate (SO_4) abundance

Globally, the two main particulate sulfate (SO_4) precursors are sulfur dioxide (SO_2) from anthropogenic sources and volcanoes, and dimethyl sulfide (DMS) from biogenic sources,

especially marine plankton. In the EM atmosphere, particulate sulfate contributes more than 50% to the submicron aerosol mass (Bardouki et al., 2003a, b; Sciare et al., 2005).

Several factors favor particulate sulfate abundance over the EM. The homogeneous conversion of gaseous SO_2 to particulate sulfate is rather slow, i.e., about 1–3% per hour (Meagher et al., 1981). Wet deposition chiefly governs the atmospheric lifetime of sulfate, estimated to be up to 6 days on a global average (Chin et al., 2000). Due to rainless conditions and associated wet deposition in summer, and the slow dry deposition velocity of sulfate aerosol (~ 0.01- 0.4 cm s^{-1}), sulfate aerosols account for 50-90% of the total sulfur in transported air masses toward the EM (Mate et al., 2002). Two additional factors favor late spring and summer particulate sulfate regional abundance. First is the intense radiant energy emitted by the sun under clear sky conditions that leads to an efficient oxidation of SO_2 to SO_4 via hydroxyl radical (OH) as the predominant oxidant during daytime (Mihalopoulos et al., 2007). Second is the prevailing summertime westerly winds that transport sulfate-rich air masses from sources over central Europe before significant removal occurs. This is consistent with Sciare et al. (2003) who measured particulate non-sea-salt SO_4 during a one-month experiment in summer 2000 at a background site on Crete, which resulted to a high average concentration of 6 µg m^{-3} (~62 nmole m^{-3}) for air masses originating from Turkey and Central Europe.

Another source of sulfate aerosols is ship emissions, which contribute substantially to atmospheric pollution over the summertime Mediterranean region. Marmer and Langmann (2005) based on a regional atmospheric-chemistry model and a radiation model found that the summer mean sulfate aerosol column burden over the Mediterranean is 7.8 mg m^{-2}, 54% originating from ship emissions.

Concentrations of sulfate-rich air masses have been measured intermittently at various downwind ground sites in Israel, the easternmost Mediterranean region, from an instrumented aircraft for a 10-year period between 1984 and 1993 by Luria et al. (1996). They found that the concentration of particulate sulfate observed during the summer was relatively high compared with other world locations. The highest values occasionally exceed 500 nmole m^{-3}. Wintertime levels were in the range of 50-100 nmole m^{-3}. In their airborne study, Wanger et al. (2000) measured an averaged SO_4 concentration of 38 ±7 nmole m^{-3} in their first series of measurement between 5 and 9 September 1993, and up to 108 ±63 nmole m^{-3} between 15 and 21 June, 1994. The annual average,

calculated in Luria et al. (1996), is 100 ±15 nmole m^{-3}, which is twice as high as predicted for the region by a global model and as high as reported for some of the most polluted regions in the USA. They pointed to several indicators suggesting that the origin of the particulate sulfate over the EM region is not from local sources but the result of LRT. The indicators include the lack of correlation between SO_4 and primary pollutants, the high SO_4 to total sulfur values, the origin of the air mass back trajectories and the fact that similar levels were observed during concurrent periods at different sites. Throughout their study, a higher concentration of SO_4 was found during the afternoon hours, especially during the summer and at the inland locations.

In another attempt to quantify the sulfur flux arriving at Israel's western coast from Europe and the Israeli pollution contribution to the air masses leaving its eastern borders towards Jordan, Matvev et al. (2002) conducted 14 research flights at an altitude of approximately 300 m above ground level, measuring sulfur dioxide and particulate sulfates during the summer and autumn seasons. Two different legs were performed for each research flight: the first over the Mediterranean Sea, west of the Israeli coast and the second along the Jordan Valley. Their results have shown that the influx of sulfur (S) reaching the Israeli coast from Europe varied in the range of 1–30 mg S h^{-1}, depending on the measuring season. The SO_4 level in the incoming LRT air masses was at least 50% of the total sulfur content. The contribution of the local pollutant sources to the outgoing easterly fluxes also varied strongly per season. The Israeli sources contributed an average of 25 mg S h^{-1} to the total pollution flux during the early and late summer as compared to only approximately 9 mg S h^{-1} during the autumn period. Synoptic analysis indicates that conditions during the summer in Israel favor the accumulation of pollution species above the MB from upwind European sources. This season is characterized by weak zonal flow within a shallow mixed layer that lead to poor ventilation rates, limiting an efficient dispersion of these pollutants during their transport eastward. Under these summer conditions, in-flux local contribution and the total out-flux of these pollutants are elevated as opposed to other seasons. To illustrate, during the autumn, the EM is usually subjected to weak easterly winds, interrupted at times by strong westerly wind flows inducing higher ventilation rates. Such autumnal meteorological conditions and the lack of major emitting sources eastwards of Israel result in lower sulfur budgets to and from Israel.

An estimate of the yearly flux showed that approximately 0.06 Tg S arrived at the Israeli coast from the west (Matvev et al., 2002). This is approximately 15% of the pollution leaving Europe

Atmos. Chem. Phys. Discuss., doi:10.5194/acp-2017-79, 2017
Manuscript under review for journal Atmos. Chem. Phys.
Discussion started: 30 March 2017

Atmospheric Chemistry and Physics Discussions

towards the EM. The outgoing flux towards Jordan contributed by local sources was calculated to be 0.13 Tg S per year, i.e. almost all the sulfur air pollution emitted in Israel. The results of the flux rates for the sulfur compounds over Israel are summarized in Table 2 for the different research flights and field campaigns. These latter results show that the uppermost fluxes from the west were for the early summer time, averaging 0.19 Tg y^{-1}. During this season, the levels doubled the averages for late summer (0.085 Tg y^{-1}) and were over five times the average levels measured for the autumn (0.035 Tg y^{-1}). The wide range in fluxes derived is explained by the varying distance from the polluted coastline

Atmos. Chem. Phys. Discuss., doi:10.5194/acp-2017-79, 2017
Manuscript under review for journal Atmos. Chem. Phys.
Discussion started: 30 March 2017

Table 2. Compilation from Rudich et al. (2008) of sulfate particulate concentrations and yearly fluxes in [a] Luria et al. (1996), [b] Wanger et al. (2000) and [c] Matvev et al. (2002).

Regions	Measurement Periods	Conc. Avg (nmole m^3)	Yearly Flux (Tg y^{-1}) (*)	Authors
Judean mountains	July-Aug. 1984,1986	86	0.08	[a]
	May-June 1989	70	0.06	
	July-Aug. 1987,1988	103	0.09	
	July-Aug. 1990	128	0.12	
	May, July 1990, 1991	85	0.08	
Sea of Galilee	Aug.-Sept. 1993	87	0.03	
	Dec. 1993	71	0.07	
North coastal plain	June 1993	106	0.12	
Eastern Mediterranean coast	Sept. 1993	38	0.08	[b]
	June 1994 (**)	108	0.22	
	June 1998	105	0.16	
	Sept. 1996	26	0.04	[c]
	Nov. 1995	21	0.03	

(*) conversion from nmole m^{-3} to yearly fluxes was along Matvev et al. (2002) taking into account the vector component of onshore wind speed, length of flight leg, and the MLD.

(**) the June 1994 flight has been performed during a highly-polluted month over Israel.

Atmos. Chem. Phys. Discuss., doi:10.5194/acp-2017-79, 2017
Manuscript under review for journal Atmos. Chem. Phys.
Discussion started: 30 March 2017

The Aerosol Optical Depth (AOD), the vertical integral over an atmospheric column of the incident light scattered and absorbed by aerosols is often used to estimate aerosol loading in the atmosphere. Nabat et al. (2013) compared AOD from several model data to satellite derived data for the period 2003-2010 over the Mediterranean region. They found that the seasonal cycle obtained from the Monitoring Atmospheric Composition and Climate (MACC) reanalysis model which includes MODIS AOD assimilation at 550 nm resembles much the satellite-derived AOD variability and have the best spatio-temporal correlation compared to AERONET stations. Based on these models and satellite derived data, Nabat et al. (2013) have clearly shown that particulate sulfate, as one of the aerosol types, has a maximum during spring and summer over the eastern MB (Fig. 16). Matvev et al. (2002) performed airborne measurements along a 150-km line west of the Israeli coast. They derived an annual flux of the order of 0.06 Tg yr^{-1} of (dry) sulfur across the corresponding surface. Given the observed ratio of sulfate to total sulfur of 40-90% in the region (Matvev et al., 2002; Sciare et al., 2003), the annual flux of SO_4 based on field measurements is 0.024-0.054 Tg y^{-1}. Rudich et al. (2008) used satellite data to estimate the pollution transport toward the EM. MODIS Terra- and Aqua-derived estimates of the annual sulfate flux along the same transect are 0.038 and 0.040 Tg y^{-1}, respectively, in the middle of the range from field observations.

Rudich et al. (2008) also found that MODIS-based estimates of the sulfate flux agree reasonably well with the Goddard Chemistry Aerosol Radiation and Transport (GOCART) model simulations of anthropogenic sulfate, as shown in Figure 17 for seasonal averages. Compared to Terra, the GOCART estimates are about 85% and 30% higher in winter and spring, respectively, but 10–25% lower in summer and autumn than the MODIS-based estimates. The annual sulfate flux from the GOCART model is 0.181 Tg y^{-1}, about 18% larger than the MODIS estimate of 0.153 Tg y^{-1}. GOCART simulations are in excellent agreement with MODIS/Aqua estimates in summer and fall, but about 50% higher in winter and spring. The GOCART simulated annual flux of 0.201 Tg y^{-1} is about 25% higher than the MODIS/Aqua estimate of 0.159 Tg y^{-1}. Based on the comparison of the two instruments, the model results, and the consistency with the aircraft measurements, they suggested that both MODIS instruments can be used for estimating the flux of pollution based on their daily AOD retrievals.

3.3 Local formation and long-range transport of total reactive nitrogen (NOy)

Research studies measuring inorganic reactive nitrogen compounds over marine areas in general, and more specifically over the EM basin are scarce (Lawrence and Crutzen, 1999; Corbett et al., 1999; Veceras et al., 2008). Measurements of nitrogen dioxide (NO_2), nitric (HNO_3) and nitrous (HNO_2) acids undertaken with instrumentation onboard a research vessel in the Aegean Sea between 25 to 29 July 2000 revealed typical NO_2 concentrations of 4–6 ppbv with a broad maximum of 20–30 ppbv. The level of NO_2 was relatively high during the night and low during the day due to enhanced photochemical activity, vertical mixing and the daily wind characteristics. Extreme NO_2 concentration were caused by up slope wind bringing air from marine traffic emissions trapped within the marine atmospheric boundary layer. The concentration of both nitric and nitrous acids in ambient air of the Aegean Sea was low, below 50 pptv. Večeřa et al. (2008) explained these results by the lack of precursors for these acids (Cohen et al., 2000), the high solar irradiation leading to HNO_3 dissociation, and the reaction of nitric acid with sodium chloride aerosol.

NOy, the total reactive nitrogen ($NO + NO_2 + HNO_3$) identified as precursors in the O_3 formation was measured by Wanger et al. (2000) during two summer airborne campaigns over the EM at an altitude of about 300 m (well within the MLD) using a high-sensitivity NO-NOy analyzer (TEII 42 S, chemiluminescence method, ±0.1 ppbv sensitivity). In the first campaign of September 1993, characterized by cleaner air mass conditions, an average NOy concentration of 1.0 ±0.6 ppbv was measured as compared to 3.9 ±1.8 ppbv sampled during the June 1994 campaign.

The Mediterranean Intensive Oxidant Study (MINOS) campaign, performed in the summer of 2001, allowed Lelieveld et al. (2002) to examine the air pollution conditions at shallow and mid-tropospheric layers over the EM Basin. During this experiment, elevated concentrations, typically 0.1 to 0.2 ppbv, of nitric oxide (NO) in the upper troposphere and only about 20 pptv within the MLD were observed at the Finokalia station.

Ranmar et al. (2002) addressed the dynamics of transboundary air pollution, where transportation emissions (such as NOx and VOC) originating from Israeli major coastal sources impact the onshore mixing layer. Their aim was to highlight the daily influence of rush-hour traffic emissions from these coasts onto the inland. They focused on the transportation sources in the Tel Aviv and Gaza Strip areas, the main coastal urban areas. This study included numerical simulations, 1994-1997 O_3 airborne measurements, and June-September ground-based measurements within 1999-

2000. A comparison of the coastal NOy spectra (Tel Aviv) to the inland NOy profiles (Modiin, 31.5°N, 35.0°E, 300 m a.s.l.) and Jerusalem discerned different dynamics for these locations. While the initial levels in Tel Aviv were higher during the morning rush hour emissions, they were subjected to a noticeable bleaching by the late morning sea breeze in comparison to inland locations, which leveled off at relatively higher midday concentrations. This may indicate, in the absence of any alternative NOy source, that the early morning NOx produced by transportation sources in Tel Aviv is transported inland, providing additional NOy to the regions along its path.

Dayan et al. (2011) measured the atmospheric concentrations of NOx in three urban centers (Tel-Aviv, Jerusalem and Beer-Sheva) in Israel before, during, and after the Day of Atonement (varying in the period September-October) for nine consecutive years (2000-2008). This permitted to inquire into the meaning and implications of local versus long-range sources of pollution and to probe the effect of meteorological conditions (synoptic systems, ventilation rates, height of surface boundary layer, and wind speed) on the level of pollution. During the Day of Atonement, all traffic and most of the industrial activities cease in the Jewish populated parts of the country. They found out that NOx concentrations during this day are significantly lower than the days before and after, reflecting NOx short residence time in the atmosphere and the strong influence of local emission sources. Moreover, the difference in concentrations of NOx in different Days of Atonement cannot be accounted for either by variations in ventilation rates, different synoptic conditions, or by height of surface boundary layer, and wind speed. They are determined by the combination of local and regional sources of emission and the meteorological conditions which control their transport from these nearby sources to the sampling station. This is consistent with Bruggemann et al. (2009) who showed that during week-days the concentrations of elemental and total carbon, certain metals, and the ultra fine (0.05-0.14 μm) and coarse (1.2-10 μm) fractions of suspended particulate matter in a German urban center are higher than during weekends when traffic density is 30% lower.

Beside cruises of research vessels, airborne campaigns, and ground truth measurements, satellite-borne initiatives have been undertaken to get a better insight on the reactive nitrogen concentrations over the EM. Marmer et al. (2009) used the OMI instrument (Boersma et al., 2007) as an observation tool to measure atmospheric NO_2 column concentrations in order to validate ship emission inventories over the MB. Figure 18 shows the average OMI NO_2 tropospheric columns (gridded to $0.125^{\circ} \times 0.125^{\circ}$) over the Mediterranean Sea for June-August 2006. The most prominent

feature here is the elevated NO_2 monthly mean. Under cloud free conditions, typical values ranged from 1.2 to 2.0 10^{15} molecules cm^{-2} over the north-eastern African coast, the EM coast, the southern coast of Turkey and the whole Aegean Sea, as compared to over 6 10^{15} molecules cm^{-2} for European inland congested regions. Based on OMI NO_2 tropospheric columns and the GEOS-Chem chemistry transport model, Vinken et al. (2014) attributed the elevated NO_2 columns regions over the Mediterranean to NO_2 emissions along ship tracks.

3.4 Carbon Monoxide sources and pathways

Carbon monoxide (CO) has a global-average lifetime of about two months in the troposphere and its molecular weight is close to that of air. This molecule is considered as an excellent tracer for pollution sources and pollution pathways through the troposphere. In addition to production by chemical oxidation in the atmosphere, CO is emitted from biomass burning, man-made sources, vegetation, and ocean. The CO seasonal cycle is mainly governed by the concentration of the hydroxyl radical (OH) in the troposphere (Novelli et al., 1992) and is expected to be the lowest in the summer when photochemistry is active and the highest during late winter or spring.

CO was measured and used as a tracer in a chemistry transport model (Lelieveld and Dentener, 2000) during the summer 2001 MINOS campaign (Lelieveld et al., 2002). The model diagnosed CO from anthropogenic sources in different parts of Europe, North America, and Asia. Trajectory calculations in the lower troposphere identified western and eastern Europe as the main source emissions. Consequently, model simulations were performed for August 2001 over Sardinia (40°N, 8°E) in the western Mediterranean (WM) and over Crete (35°N, 25°E). Considering the negligible impact of local pollution sources, the high CO levels observed over Crete, in excess of 150 ppbv, were surprising. The model results indicated that regions surrounding the Mediterranean such as southern Italy, Greece, Serbia, Macedonia, the Middle East, and North Africa contribute relatively little to the CO pollution, typically about 20%. Furthermore, Lelieveld et al. (2002) found that the EM is affected by CO polluted air emitted from Eastern Europe, Poland, the Ukraine, and Russia. This pollution flow, east of the Carpathian Mountains, is channeled over the Black Sea and the Aegean Sea, and contributes 60 to 80% of the boundary-layer CO over the EM. Their model results are consistent with aircraft measurements, showing that the entire Mediterranean lower troposphere is polluted.

In the free troposphere, where westerly winds predominate, they revealed a quite different situation as compared to concentrations measured within the MLD. The mid-tropospheric CO measurements were ~75-80 ppbv. From their model tracer analysis, the largest contribution over the Mediterranean is found originating from Asia (40 to 50%). The CO typical lifetime (~2 months) enables air mass to circumnavigate the globe which results in a low variability of its concentrations. Lelieveld et al. (2002) found that contributions by pollution from western and eastern Europe to mid-tropospheric CO were only about 10%.

Drori et al. (2012) conducted a study to locate the various CO sources converging from Europe, North Africa and the Middle East and quantify their respective contributions to the EM. Background CO concentrations are monitored regularly over the southern part of Israel in Sde-Boker (WIS Station Negev Desert: 31.13°N, 34.88°E, 400 m) as part of the NOAA Earth System Research Laboratory Global Monitoring Division (ESRL/GMD) which aims at representing the EM. While comparing the seasonal cycle of Sde-Boker to other European ESRL/GMD background sites (see Table 3), one essential feature is eminent from their results represented in Figure 19: CO concentrations are high over winter months, decreasing abruptly during April and increasing again from November. A second maximum is observed during August compared to July and September (Drori et al., 2012).

Table 3. Locations and elevations of ESRL/GMD sites

Code	Name	Latitude	Longitude	Elevation (m)	Country
WIS	WIS Station Negev Desert	31.13	34.88	400.0	Israel
HUN	Hegyhatsal	46.95	16.65	248.0	Hungary
LMP	Lampedusa	35.52	12.62	45.0	Italy
BSC	Black Sea Constanta	44.17	28.68	3.0	Romania
OXK	Ochsenkopf	50.03	11.80	1022.0	Germany
BAL	Baltic Sea	55.35	17.22	3.0	Poland
MHD	Mace Head County Galway	53.33	−9.90	5.0	Ireland

Atmos. Chem. Phys. Discuss., doi:10.5194/acp-2017-79, 2017
Manuscript under review for journal Atmos. Chem. Phys.
Discussion started: 30 March 2017

To get an insight on the spatial distribution of CO concentrations over the EM, the Version 4 MOPITT level-2 CO retrievals (Deeter et al., 2010) were employed by Drori et al. (2012) using a priori information for MOPITT V4 CO retrievals based on MOZART simulation climatology. While in-situ measurements represent a small volume at a specific layer, MOPITT retrievals can be regarded as averaged value over several layers (e.g. the 900 hPa retrieval is averaged from the surface up to the 700 hPa level). The averaging kernel profile obtained for two retrievals near Sde-Boker ESRL/GMD station shows that, during the day, the 900 hPa retrieval sharply peaks at the same level, indicating that there is a good sensitivity to lower tropospheric concentration. During the night, the 900 hPa retrieval moderately peaks at its level with the same contribution from the 800 hPa level pointing at a slightly less sensitivity to the lower tropospheric concentration (not shown).

The anomalous high concentration observed at the WIS ESRL/GMD Sde-Boker station, and calculated by the MOZART-4 chemistry-transport model during August (Fig. 19), might be limited to lower levels, and therefore averaging over several layers might hide this signal. MOPITT retrievals are highly variable both temporally and spatially, especially during winter and spring. This variability stems from the highly variable boundary layer height (300–2000 m) featuring the spring and cold fronts sweeping the EM during winter.

Furthermore, Drori et al. (2012) compared the in-situ measurements at Sde-Boker and CO retrieved from MOPITT to a chemical transport model. For this sake, the MOZART-4 global chemical transport model of the troposphere (Emmons et al., 2010) was used. CO sources included direct emissions and secondary production from hydrocarbons oxidation, while CO sinks included a reaction with OH and dry deposition. The seasonal cycle of surface CO at Sde-Boker simulated by MOZART averaged for five consecutive years shows a similar pattern exhibiting high CO concentration during winter months, reaching a maximum in spring, and decreasing sharply around May. The CO concentration in mid-summer months (i.e., July and August) surpasses those of the early summer (i.e., May–June) (Fig. 19).

To attribute the CO sources affecting the EM, Drori et al. (2012) partitioned these sources using a tagging method into five types: anthropogenic, biogenic, fire, chemical production and ocean. The total and specific sources 2006–2007 times-series of MOZART CO concentration at 30° N and 33.75° E are shown in Figure 20, except for ocean, that are negligible and thus not shown. Both

biogenic (green line) and biomass burning sources (red line) have a minor contribution. Biogenic sources are characterized by a distinct seasonal cycle with high contribution over winter and low daily variability. Biomass burning has no defined seasonal signature and contributes on an episodic event basis. CO from chemical production (orange) contributes substantially (50–80 ppb) with a defined seasonal cycle: low during winter and autumn and high during summer featured by a low daily variability. Anthropogenic sources were found to be the main contributor to the total CO (purple, 50–180 ppb). As expected, their seasonal cycle is featured by winter elevated concentrations decreasing during spring, slightly increasing during summer; and decreasing again during autumn. The daily variability is high and similar to the total CO daily variability. Comparing the daily variability of the various sources, Drori et al. (2012) concluded that anthropogenic sources mainly govern total CO daily variability over the EM.

To further attribute the CO surface daily variation, Drori et al. (2012) tagged the anthropogenic sources for the three northern continents, i.e., North America, Europe, and Asia. Figure 21 shows the results of these anthropogenic sources attribution to the CO surface. European anthropogenic sources contribute substantially (10–80 ppb) to local CO concentrations with the greatest daily variability all year round. Asian and North American sources are in the same order of magnitude (10–25 ppb) with low daily variability during most of the year, and very small variability during summer. Obviously, daily summer CO variations in the EM are mainly caused by European anthropogenic sources. The seasonal cycle of the European contribution is very similar to the seasonal cycle of total CO, featured by a high concentration in winter, spring, and autumn and a lower summer concentration. The contribution of European emissions to CO surface concentrations is comparable to that from EM local emissions.

Drori et al. (2012) found, however, that local and European emission contributions to local CO concentrations are generally negatively correlated, meaning that either local or European sources are dominant, except during summer, when both sources affect simultaneously the local CO concentration. A possible explanation for the positive summer correlation might be explained by the short range of air mass transport caused by the dominant summer synoptic system, i.e., the Persian trough in its weak mode recirculating local and European emissions, and by the fact that summer chemical production is a major CO source over the EM.

Another recent modeling study focused on CO concentrations was conducted by Myriokefalitakis et al., (2016). They compared and validated model results against in-situ observations at the surface, in the MLD and in the free troposphere (between 850 hPa and the tropopause) in the countryside and remote atmosphere over Europe for 2008. This study analyzes the total CO budget and the partial contribution of regional anthropogenic, biogenic and biomass burning CO emissions in the EM. The budget calculated for 2008 in the EM MLD, using a basic simulation relying on anthropogenic emissions and meteorology, points at a load of 0.6 Tg of CO, a chemical production of 10 Tg yr^{-1}, primary emissions in the region of 8 Tg yr^{-1} and a dry deposition flux of 3 Tg yr^{-1}. Moreover, Myriokefalitakis et al (2016) found that subsidence from higher atmospheric layers typifying the EM summer is an important CO source (12 Tg yr^{-1}) in the EM free troposphere. At the surface, anthropogenic local emissions in the EM was found to contribute by 18% to surface CO levels on an annual average. Over Cairo, out of the total surface CO concentration, roughly 32% are contributed by anthropogenic sources. These EM CO concentration results are consistent with previous modelling studies (e.g., Kanakidou et al., 2011; Drori et al., 2012; Im and Kanakidou, 2012).

3.5 Methane concentrations

CH_4 concentration in the atmosphere is of natural and anthropogenic origins. It is the most affecting greenhouse gas after water vapor and CO_2 due to its high global warming potential as contributed by its infrared absorption and long atmospheric lifetime. CH_4 emissions are primarily caused by microbiological decay of organic matter under depleted of dissolved oxygen conditions in wetlands, followed by decomposition of solid waste and enteric fermentation from domestic livestock. As for the geologic sources, a total geological CH_4 flux of 53 ±11 Tg yr^{-1} was suggested, which accounts for 7–10% of the total global CH_4 budget (Etiope et al., 2008). The geological formations contributing to CH_4 over the Greater Area of the EM (25° N- 50° N, 5° E- 55 °E) are mud volcanoes with essential hot spots located over eastern Romania, the Black Sea, Central and Eastern Azerbaijan and the Caspian Sea.

Georgoulias et al. (2011) used data from the SCIAMACHY (Scanning Imaging Absorption Spectrometer for Atmospheric Cartography) instrument on board the European environmental satellite ENVISAT (Bovensmann et al., 1999). SCIAMACHY's spectral near-infrared nadir measurements are sensitive to CH_4 and CO_2 concentration changes at all atmospheric altitudes,

including the MLD where the signal emitted from the surface source is the largest. Annual, seasonal and monthly spatial distribution of CH_4 were displayed for 2003 and 2004 based on the analysis of Weighting Function Modified Differential Optical Absorption Spectroscopy (WFM-DOAS) version 1.0 (Schneising et al., 2009) dry air column-averaged mole fractions, denoted as XCH_4 (ppb). The reflectivity of water surfaces is very low, therefore Georgoulias et al. (2011) presented their results over land only by depicting the concentration of CH_4 along the coasts of the EM Basin. To reduce the noise inserted by the single pixel retrieval error and the temporal and spatial sparsity of the data, the data were averaged on $1^{\circ} \times 1^{\circ}$ monthly mean grids. Annual, summer and August spatial distributions for 2003 are displayed on Fig. 22 top, mid and bottom panel, respectively.

Those maps illustrate an eminent seasonal variation with a summer maximum in XCH_4 levels observed in both consecutive years (2004 not shown). The northeastern African coast exhibits the highest XCH_4 values, with a hot spot over the Nile's delta in Egypt in summer and August. The lowest XCH_4 levels along the Arabian Peninsula, the Zagros Mountain and eastern Anatolia mountain barrier coincide spatially with high altitude areas. To examine to what extent the warm period affects the annual, seasonal, and latitudinal patterns, Georgoulias et al. (2011) further proceeded to a monthly analysis. They observed an increase in XCH_4 levels during the summer season, August being the month with the highest levels of 1775-1780 ±24 ppb for both 2003 and 2004. The highest values are concentrated in the northeastern part of the area primarily in July-August. From July to September, there is a shift of high XCH_4 levels from higher to lower latitudes. Despite the abundance of mud volcanoes over the Greater Area of the Eastern Mediterranean region, Georgoulias et al. (2011) ruled out the possibility that the CH_4 total columns from SCIAMACHY (2003-2004) measured over these EM regions were attributed to volcano eruptions.

Ricaud et al. (2014) presented a thorough analysis of atmospheric CH_4 distributions over the MB in the troposphere, as part of the Chemical and Aerosol Mediterranean Experiment (ChArMEx) program, using both satellite measurements and model simulations. For this sake, they analyzed space-borne measurements from (i) the Thermal And Near infrared Sensor for carbon Observations-Fourier Transform Spectrometer (TANSO-FTS) instrument on the Greenhouse gases Observing SATellite (GOSAT) satellite, (ii) the Atmospheric InfraRed Spectrometer (AIRS) on the AURA platform and (iii) the Infrared Atmospheric Sounder Interferometer (IASI)

instrument aboard the MetOp-A platform. These space-borne tools were used in conjunction with the results obtained from three global models: the Chemical Transport Model (CTM) MOCAGE (Teyssedre et al., 2007), the Chemical Climate Models (CCMs) CNRM-AOCCM, (Michou et al., 2011) and LMDz-OR-INCA (Hourdin et al.,2006).

The sensitivity of the space-borne sensors is mainly located in the upper tropospheric layers peaking around 300 hPa with an envelope as defined by the half-width at half-maximum of the averaging kernels (see Figure 23) from 400 to 200 hPa. Consequently, the comparisons between measurements and model outputs of CH_4 is mainly concentrated on the layer around 300 hPa for AIRS and GOSAT, or considering the total column for IASI.

In summer, the horizontal distribution of CH_4 in the upper troposphere shows a clear longitudinal gradient between the East and the West of the Mediterranean Basin, both in the space-borne measurements and in the model calculations (Figure 24). There is a maximum of CH_4 in the Eastern MB compared to the Western MB, both considering the upper tropospheric layer and the total column information. The difference between the East and the West of the MB has been calculated within all the datasets and the seasonal variations has been investigated (Figure 25). This clearly shows that the East-West difference peaks in summer, mainly in August.

The long-range transport conditions in the upper troposphere differ over both parts of the Mediterranean Basin. In the western part, whatever the season considered, air masses are basically coming from the west. However, in the EM, apart from the westerlies influence, air masses are also originating from Northern Africa and the Arabic Peninsula (Ziv et al., 2004; Liu et al., 2009), and even farther away, from Asia.

To further examine the origin of air masses reaching the Eastern MB, a six-day back-trajectory from the point at 33°N, 35°E located in the EM (red filled circle in Fig. 26) was calculated, considering vertical movement, using the British Atmospheric Data Centre (BADC) trajectory service (http://badc.nerc.ac.uk/community/trajectory/) for July-August over 2001-2010 every 12 hours. The position of the gravity center of all trajectories (i.e. the maximum in the probability density function) is displayed every 24 h in Figure 26 at 850 (red stars), 700 (orange), 500 (green), 300 (blue) and 200 hPa (yellow). For this purpose, data from ECMWF archive (2.5 degree/pressure levels) were used in the calculation.

Based on these studies focused on the EM, Ricaud et al. (2014) proposed a scheme displaying the transport mechanism (Fig. 27) representing the several stages process: (1) capturing of lower tropospheric pollutants, including CH_4, in the Asian monsoon; (2) pollutants ascent to the upper troposphere by the Asian monsoon ; (3) accumulation of pollutants within the Asian monsoon in the upper troposphere; (4) long- range transport and large-scale repartition of pollutants in the upper troposphere from the Asian Monsoon Anticyclone (AMA) to the Middle East and North Africa; (5) Subsiding air masses yielding to the build-up of pollutants at mid-tropospheric layers above the EM.

4. Conclusions and Perspectives

This review demonstrates the significant progress made in understanding the atmospheric pollution over the MB. Measurements from space-borne and aircraft instruments and outputs from chemistry-climate models and chemistry transport models clearly revealed that the general atmospheric dynamic summer conditions characterizing the eastern MB differ much from the western ones. The impact of the different meteorological regimes together with the seasonal variabilities of the emissions of various atmospheric pollutants result in a longitudinal gradient between the eastern and the western MBs.

Several new campaigns have been recently organized to give more insights in the understanding of the processes occurring in the Eastern and Western parts of this basin. The TRAnsport and Air Quality (TRAQA) campaign (Attié et al., 2014) held in 2012-2014 was dedicated to the export/import of pollutants from the French continent to the Mediterranean Sea by means of balloon and airborne measurements. The Gradient in Longitude of Atmospheric constituents above the Mediterranean basin (GLAM) campaign (Ricaud et al., manuscript submitted) held in August 2014 was dedicated to the study of the gradient of chemical constituents (pollutants and greenhouse gases) from Toulouse (France) to Larnaca (Cyprus) and the impact of the AMA on the EM pollutant levels.

Surface background stations in the Eastern MB (e.g., Crete, Greece and Larnaca, Cyprus) and in the Western MB (e.g., Menorca, Spain and Lampedusa, Italy) deployed even more instruments to obtain a wide variety of atmospheric parameters (meteorology, chemistry, dynamics, radiation, etc.). These campaigns were organized in close relationship with modelling studies (forecasts, and

re-analyses) and space-borne observations. New airborne campaigns are under analysis, e.g. OMO in summer 2015, or in project (RIMES in summer 2018) in order to quantify the export of the Asian pollutants to the EM basin chemical constituents loading.

Concurrently to these intensive experiments, new sites have been instrumented. In early 2015, the Agia Marina Xyliatou EMEP rural background air quality station sited at 532 m in altitude in the center of Cyprus (35°02'17"N, 33°03'28"E), and operated since October 1996 (Kleanthous et al., 2014), has been augmented with a package of atmospheric chemistry and physics monitoring instruments thanks to the Cyprus Institute and French laboratories, in order to initiate an enhanced atmospheric chemistry observation period of several years in the easternmost MB. Unmanned aircraft vehicles are also deployed on a regular basis to document the lower troposphere above the station and the German TROPOS institute has deployed a full set of aerosol-cloud-water vaper remote sensing instrument for almost a year in October 2016. This unprecedented experimental effort is expected to bring information on the variability of new compounds and processes with a focus on VOCs and secondary and carbonaceous aerosols and their origins, and on interactions between aerosols and the water vapor cycle.

References

Akritidis, D., Zanis, P., Pytharoulis, I., Mavrakis, A., and Karacostas, Th.: A deep stratospheric intrusion event down to the earth's surface of the megacity of Athens, Meteorol. Atmos. Phys., 109, 9–18, doi:10.1007/s00703-010-0096-6, 2010.

Alper-Siman Tov, D., Peleg, M., Matveev, V., Mahrer, Y., Seter, I., and Luria, M.: Recirculation of polluted air masses over the east Mediterranean coast, Atmos. Environ., 31, 1441-1448, doi:10.1016/S1352-2310(96)00321-4, 1997.

Andreae, M. O.: The dark side of aerosols, Nature, 409, 671-672, doi :10.1038/35055640, 2001.

Angevine, W. M., Hare, J. E., Fairall, C. W., Wolfe, D. E., Hill, R. J., Brewer, W. A., and White, A. B.: Structure and formation of the highly stable marine boundary layer over the Gulf of Maine, J. Geophys. Res., 111, D23S22, doi:10.1029/2006JD007465, 2006.

Attié, J. L., Ravetta, F., Durand, P., El Amraoui, L., Di Biaggio, C., Dulac, F., Sicard, M., Renard, J.B., Fleury, L., Bourdon, A., Verdier, N., and the TRAQA/ChArMEx Team: Transport of Pollution and Air Quality experiment over the Mediterranean basin (TRAQA/ChArMEx campaign), Geophys. Res. Abstr., 16, EGU2014-12125, 2014, EGU General Assembly 2014.

Bardouki, H., Berresheim, H., Vrekoussis, M., Sciare, J., Kouvarakis, G., Oikonomou, K., Schneider, J., and Mihalopoulos, N.: Gaseous (DMS, MSA, SO_2, H_2SO_4, and DMSO) and particulate (sulfate and methanesulfonate) sulfur species over the northeastern coast of Crete, Atmos. Chem. Phys., 3, 1871–1886, doi:10.5194/acp-3-1871-2003, 2003a.

Bardouki, H., Liakakou, H., Economou, C., Smolik, J., Zdimal, V., Eleftheriadis, K., Lazaridis, M., and Mihalopoulos, N.: Chemical composition of size resolved atmospheric aerosols in the eastern Mediterranean during summer and winter, Atmos. Environ., 37, 195–208, doi:10.1016/S1352-2310(02)00859-2, 2003b.

Barkan, J., and Feliks, Y.: Observations of the diurnal oscillation of the inversion over the Israeli coast, Boundary-Layer Meteorol., 62, 393-409, doi:10.1007/BF00705568, 1993.

Berman, S., Ku, Y. J., and Rao, S. T.: Spatial and Temporal Variation in the Mixing Depth over the Northeastern United States during the Summer of 1995, J. Appl. Meteorol., 38, 1661-1673, doi:10.1175/1520-450(1999)038<1661: SATVIT>2.0.CO;2 1999.

Boersma, K. F., Eskes, H. J., and Brinksma, E. J.: Error analysis for tropospheric NO2 retrieval from space, J. Geophys. Res., 109, D04311, doi :10.1029/2003JD003962, 2004.

Bovensmann, H., Burrows, J. P., Buchwitz, M., Frerick, J., Noel, S., Rozanov, V. V., Chance, K. V., and Goede, A.P.H.: SCIAMACHY: mission objectives and measurement modes, J. Atmos. Sci., 56, 127–150, doi:10.1175/1520-0469(1999)056<0127: SMOAMM>2.0.CO;2 1999.

Bruggemann, E., Gerwig, H., Gnauk, T., Muller, K., and Herrmann, H.: Influence of seasons, air mass origin and day of the week on size-segregated chemical composition of aerosol particles at a kerbside, Atmos. Environ., 43, 2456-2463, doi: 10.1016/j.atmosenv.2009.01.054, 2009.

1 Chin, M., Rood, R. B., Lin, S. J., Muller, J. F., and Thompson, A. M.: Atmospheric sulfur cycle
2 simulated in the global model GOCART: Model description and global properties, J.
3 Geophys. Res., 105, 24,671–24,687, doi :10.1029/2000JD900384, 2000.

4 Cohen, R. C., Perkins, K. K., Koch, L. C., Stimpfle, R. M., Wennberg, P. O., Hanisco, T. F.,
5 Lanzendorf, J.E., Bonne, G. P., Voss, P. B., Salawitch, R. J., Del Negro, L. A., Wilson, J.
6 C., McElroy, C.T., and Bui, T. P.: Quantitative constraints on the atmospheric chemistry
7 of nitrogen oxides: An analysis along chemical coordinates, J. Geophys. Res., 105, 24283–
8 24304, doi :10.1029/2000JD900290, 2000.

9 Corbett, J. J., Fischbeck, P. S., and Panis, S. N.: Global nitrogen and sulfur inventories for ocean-
10 going ships, J. Geophys. Res., 104, 3457–3470, doi :10.1029/1998JD100040, 1999.

11 Daskalakis, N., Myriokefalitakis, S., and Kanakidou, M.: Sensitivity of tropospheric loads and
12 lifetimes of short lived, Atmos. Chem. Phys., 15, 3543–3563, doi :10.5194/acp-15-3543-
13 2015.

14 Dastoor, A. P., and Larocque, Y.: Global circulation of atmospheric mercury: a modeling study,
15 Atmos. Environ., 38, 147-161, doi: 10.1016/j.atmosenv.2003.08.037, 2004.

16 Davis, R. E., and Kalkstein, L. S.: Using a spatial synoptic classification to assess changes in
17 atmospheric pollution concentrations, Phys. Geogr., 11, 320-342, 1990.

18 Dayan, U. 1986: Climatology of back trajectories from Israel based on synoptic analysis. J.
19 Climatol. Appl. Meteorol., 25, 591-595, doi:10.1175/1520-0450(1986)025<0591:
20 COBTFI>2.0.CO;2, 1986.

21 Dayan, U., and Graber, M.: Analysis of synoptic conditions in the eastern Mediterranean that led
22 to elevated air pollution concentration in Israel, in Developments in Arid Zone Ecology
23 and Environmental Quality, Shuval, H. I. (Ed.), Balaban International Science Services,
24 PA, 383–391, 1981.

25 Dayan U., and Koch, J.: Ozone concentration profiles in the Los Angeles Basin - A possible
26 similarity in the build-up mechanism of inland surface ozone in Israel, J. Appl. Meteorol.,
27 35, 1085-1090, doi:10.1175/1520-0450(1996)035<1085: OCPITL>2.0.CO;2, 1996.

Dayan, U., and Levy, I.: Relationship between synoptic-scale atmospheric circulation and ozone concentrations over Israel, J. Geophys. Res., 107, D24, 4813, doi:2002JD002147, 2002.

Dayan U., and Rodnizki, J.: The temporal behavior of the atmospheric boundary layer in Israel, J. Appl. Meteorol., 38, 830-836, doi:10.1175/1520-0450(1999)038<0830: TTBOTA>2.0.CO;2., 1999.

Dayan, U., Shenhav, R., and Graber, M.: The spatial and temporal behavior of the mixed layer in Israel, J. Appl. Meteorol., 27, 1382–1394, doi:10.1175/1520-0450(1988)027<1382: TSATBO>2.0.CO;2, 1988.

Dayan, U., Heffter, J., Miller, J., and Gutman, G.: Dust intrusion events into the Mediterranean Basin. J. Appl. Meteorol., 30, 1185-1199, doi:10.1175/1520-0450(1991)030<1185: DIEITM>2.0.CO;2, 1991.

Dayan, U., Heffter, J., and Miller, J.: Seasonal distribution of the boundary layer depths over the Mediterranean Basin, in Guerzoni, S., and Chester, R. (Eds.), The Impact of Desert Dust Across the Mediterranean, 103-112, Kluwer, Dordrecht, 1996.

Dayan, U., Lifshitz-Goldreich, B., and Pick, K.: Spatial and structural variation of the atmospheric boundary layer during summer in Israel─Profiler and rawinsonde measurements, J. Appl. Meteorol., 41, 447-457, doi:10.1175/1520-0450(2002)041<0447: SASVOT>2.0.CO;2., 2002.

Dayan, U., Ziv, B., Shoob, T., and Enzel, Y.: Suspended dust over southeastern Mediterranean and its relation to atmospheric circulations, Int. J. Climatol., 28, 915-924, doi:10.1002/joc.1587, 2008.

Dayan, U., Erel, Y., Shpund, J., Kordova, L., Wanger, A., and Schauer, J. J.: The impact of local sources and meteorological factors on nitrogen oxide and particulate matter concentrations: A case study of the Day of Atonement in Israel, Atmos. Environ., 45, 3325-3332, doi: 10.1016/j.atmosenv.2011.02.017, 2011.

Deeter, M. N., Edwards, D. P., Gille, J. C., Emmons, L. K., Francis, G., Ho, S.-P., Mao, D., Masters, D., Worden, H., Drummond, J.R., and Novelli, P. C.: The MOPITT Version 4 CO

Product: Algorithm enhancements, validation, and long-term stability, J. Geophys. Res., 115, D07306, doi :10.1029/2009JD013005, 2010.

Doche, C., Dufour, G., Foret, G., Eremenko, M., Cuesta, J., Beekmann, M., and Kalabokas, P.: Summertime tropospheric-ozone variability over the Mediterranean basin observed with IASI, Atmos. Chem. Phys., 14, 10589–10600, doi:10.5194/acp-14-10589-2014, 2014.

Drori, R., Dayan, U., Edwards, D. P., Emmons, L. K., and Erlick, C.: Attributing and quantifying carbon monoxide sources affecting the Eastern Mediterranean: A combined satellite, modelling, and synoptic analysis study, Atmos. Chem. Phys. 12, 1067-1082, doi:10.5194/acp-12-1067-2012, 2012.

Emmons, L. K., Walters, S., Hess, P. G., Lamarque, J.-F., Pfister, G. G., Fillmore, D., Granier, C., Guenther, A., Kinnison, D., Laepple, T., Orlando, J., Tie, X., Tyndall, G., Wiedinmyer, C., Baughcum, S. L., and Kloster, S.: Description and evaluation of the Model for Ozone and Related Chemical Tracers, version 4 (MOZART-4), Geosci. Model Dev., 3, 43–67, doi:10.5194/gmd-3-43-2010, 2010.

Erel, Y., Axelrod, T., Veron, A., Mahrer, Y., and Dayan, U.: Trans-boundary atmospheric lead pollution, Environ. Sci. Technol., 36, 3230-3233, doi:10.1021/es020530q, 2002.

Erel, Y., Kalderon-Asael, B., Dayan, U., and Sandler, A.: European pollution imported by cooler air masses to the eastern Mediterranean during the summer, Environ. Sci. Technol., 41, 5198-5203, doi:10.1021/es062247n, 2007.

Erel, Y., Tirosh, O., Kessler, N., Dayan, U., Belkin, S., Stein, M., Sandler, A., and Schauer, J. J.: Atmospheric particulate matter (PM) in the Middle East: Toxicity, transboundary transport, and influence of synoptic conditions, in Censi, P., Darrah, T., and Erel, Y. (Eds.), Medical Geochemistry: Geological Materials and Health, doi:10.1007/978-94-007-4372-43, Springer, Dordrecht, 2013.

Etiope, G., Lassey, K.R., Lusman, K., and Oschi, B.: Re-appraisal of the fossil methane budget and related emission from geologic sources, Geophys. Res. Lett., 35, L09307, doi:10.1029/2008GL033623, 2008.

Feliks, Y.: A numerical model for the estimation of the diurnal fluctuation of the inversion due to the sea breeze, Boundary-Layer Meteorol., 62, 151-161, doi:10.1007/BF00705552, 1992.

Galani, E., Balis, D., Zanis, P., Zerefos, C., Papayannis, A., Wernli, H., and Gerasopoulos, E.: Observations of stratosphere-troposphere transport events over the eastern Mediterranean using a ground-based lidar system, J. Geophys. Res., 108, 8527, doi:10.1029/2002JD002596, 2003.

Gamo, M., Yamamoto, S., and Yokoyama, O.: Airborne measurements of the free convective internal boundary layer during the sea breeze, J. Meteor. Soc. Japan, 60, 1284–1298, 1982.

Georgoulias, A. K., Kourtidis, K. A., Buchwitz, M., Schneising, O., and Burrows, J. P.: A case study on the application of SCIAMACHY satellite methane measurements for regional studies: the greater area of the Eastern Mediterranean, Int. J. Remote Sens., 32, 787-813, doi:10.1080/01431161.2010.517791, 2011.

Gerasopoulos, E., Kouvarakis, G., Vrekoussis, M., Kanakidou, M., and Mihalopoulos, N.: Ozone variability in the marine boundary layer of the eastern Mediterranean based on 7-year observations, J. Geophys. Res., 110, D15309, doi :10.1029/2005JD005991, 2005.

Glaser, E., Dagan, N., Furer, O., Gamliel, M., Yogev, A., Fastig, S., Dayan, U., and Benayahu, Y.: A comparison of balloon soundings and lidar scans for measuring the height of the turbulent mixed-layer at a coastal site in Israel, Water Sci. Technol., 27, 271-278, 1993.

Gryning, S. E.: The Oresund experiment—A Nordic mesoscale dispersion experiment over a land-water-land area, Bull. Amer. Meteorol. Soc., 66, 1403–1407, doi:10.1175/1520-0477(1985)066<1403: TENMDE>2.0.CO;2, 1985.

Halevy, G., and Steinberger, E. H.: Inland penetration of the summer inversion from the Mediterranean coast in Israel, Isr. J. Earth Sci., 23, 47-54, 1974.

Hansen, J., Lacis, A., and Prather, M.: Greenhouse effect of chlorofluorocarbons and other trace gases, J. Geophys. Res., 94, 16417-16421, doi:10.1029/JD094iD13p16417, 1989.

Harpaz, T., Ziv, B., Saaroni, H., and Beja, E.: Extreme summer temperatures in the East Mediterranean—dynamical analysis, Int. J. Climatol., 34, 849–862. doi:10.1002/joc.3727, 2014.

Harris, J. M.: The GMCC atmospheric trajectory program, NOAA Tech. Memo. ERL-ARL-116, 30 pp., 1982.

Hein, R., Dameris, M., Schnadt, C., Land, C., Grewe, V., Kohler, I., Ponater, M., Sausen, R., Steil, B. B., Landgraf, J., and Bruhl, C.: Results of an interactively coupled atmospheric chemistry–general circulation model: Comparisons with observations, Ann. Geophys., 19, 435-457, doi:10.5194/angeo-19-435-2001, 2001.

Holtslag, A. A. M., and Van Ulden, A. P.: A simple scheme for daytime estimates of the surface fluxes from routine weather data, J. Climate Appl. Meteorol., 22, 517–529, doi:10.1175/1520-0450(1983)022<0517: ASSFDE>2.0.CO;2, 1983.

Hourdin, F., Musat, I., Bony, S., Braconnot, P., Codron, F., Dufresne, J. L., Fairhead, L., Filiberti, M. A., Friedlingstein, P., Grandpeix, J. Y., Krinner, G., LeVan, P., Li, Z. X., and Lott, F.: The LMDZ4 general circulation model: climate performance and sensitivity to parametrized physics with emphasis on tropical convection, Clim. Dyn., 27, 787–813, doi: 10.1007/s00382-006-0158-0, 2006.

James, P., Stohl, A., Forster, C., Eckhardt, S., Seibert, P., and Frank, A.: A 15-year climatology of stratosphere–troposphere exchange with a Lagrangian particle dispersion model, 2, Mean climate and seasonal variability, J. Geophys. Res., 108, 8522, doi:10.1029/2002JD002639, 2003.

Kalnay, E., Kanamitsu, M., Kistler, R., Collins, W., Deaven, D., Gandin, L., Iredell, M., Saha, S., White, G., Woollen, J., Zhu, Y., Leetmaa, A., Reynolds, B., Chelliah, M., Ebisuzaki, W., Higgins, W., Janowiak, J., Mo, K. C., Ropelewski, C., Wang, J., Jenne, R., and Joseph, D.: The NCEP/NCAR 40-year reanalysis project, Bull. Am. Meteorol. Soc., 77, 437–472, doi:10.1175/1520-0477(1996)077<0437: TNYRP>2.0.CO;2, 1996.

Kalthoff, N., Binder, H. J., Kossman, M., Vogtlin, R., Corsmeier, U., Fiedler, F., and Schlager, H.: Temporal evolution and spatial variation of the boundary layer over complex terrain, Atmos. Environ., 32, 1179–1194, doi:10.1016/S1352-2310(97)00193-3, 1998.

Kanakidou, M., Mihalopoulos, N., Kindap, T., Im, U., Vrekoussis, M., Gerasopoulos, E., Dermitzaki, E., Unal, A., Koçak, M., Markakis, K., Melas, D., Kouvarakis, G., Youssef, A. F., Richter, A., Hatzianastassiou, N., Hilboll, A., Ebojie, F., Wittrock, F., von Savigny, C., Burrows, J. P., Ladstaetter-Weissenmayer, A., and Moubasher, H.: Megacities as hot spots of air pollution in the East Mediterranean, Atmos. Environ., 45, 1223–1235 doi:10.1016/j.atmosenv.2010.11.048, 2011.

Kistler, R., Kalnay, E., Collins, W., Saha, S., White, G., Woollen, J., Chelliah, M., Ebisuzaki, W., Kanamitsu, M., Kousky, V., van den Dool, H., Jenne, R., and Fiorino, M.: The NCEP/NCAR 50-year reanalysis: monthly means CD-ROM and documentation, Bull. Am. Meteorol. Soc., 82, 247–267, doi10.1175/1520-0477(2001)082<0247: TNNYRM>2.3.CO;2, 2001.

Kleanthous, S., Vrekoussis, M., Mihalopoulos, N., Kalabokas, P., and Lelieveld, J.: On the temporal and spatial variation of ozone in Cyprus, Sci. Total Environ., 476-477, 677-687, doi: 10.1016/j.scitotenv.2013.12.101, 2014.

Kley, D.: Tropospheric chemistry and transport, Science, 276, 1043–1045, doi:10.1126/science.276.5315.1043, 1997.

Koch, J., and Dayan, U.: A synoptic analysis of the meteorological conditions affecting dispersion of pollutants emitted from tall stacks in the coastal plain of Israel, Atmos. Environ., 26, 2537–2543, doi:10.1016/0960-1686(92)90105-T, 1992.

Kourtidis, K., Cerefos, C., Rapsomanikis, S., Simeonov, C., Balis, D., Perros, P. E., Thompson, A. M., Witte, J., Calpini, B., Sharobiem, W. M., Papayannis, A., Mihalopoulos, N., and Draku, R.: Regional levels of ozone in the troposphere over eastern Mediterranean, J. Geophys. Res., 107, 8140, doi :10.1029/2000JD000140, 2002.

Kouvarakis, G., Vrekoussis, M., Mihalopoulos, N., Kourtidis, K., Rappenglueck, B., Gerasopoulos, E., and Zerefos, C.: Spatial and temporal variability of tropospheric ozone

(O_3) in the boundary layer above the Aegean Sea (eastern Mediterranean), J. Geophys. Res., 107, 8137, doi :10.1029/2000JD000081, 2002.

Kuwagata, T., Masuko, N., Sumioka, M., and Kondo, J. : The daytime PBL heating process over complex terrain in central Japan under fair and calm weather conditions. Part II: Regional heat budget, convective boundary layer and surface moisture availability, J. Meteor. Soc. Japan, 68, 639–650, 1990.

Lashof, D. A., and Ahuja, D. R.: Relative contributions of greenhouse gas emissions to global warming, Nature, 344, 529-531; doi:10.1038/344529a0, 1990.

Lawrence, M. G., and Crutzen, P. J.: Influence of NOx emissions from ships on tropospheric photochemistry and climate, Nature, 402, 167–170, doi:10.1038/46013, 1999.

Lelieveld, J., and Dentener, F. J.: What controls tropospheric ozone? J. Geophys. Res., 105, 3531-3551, doi:10.1029/1999JD901011, 2000.

Lelieveld, J., Berresheim, H., Borrmann, S., Crutzen, P. J., Dentener, F. J., Fischer, H., Feichter, J., Flatau, P. J., Heland, J., Holzinger, R., Korrmann, R., Lawrence, M. G., Levin, Z., Markowicz, K. M., Mihalopoulos, N., Minikin, A., Ramanathan, V., de Reus, M., Roelofs, G. J., Scheeren, H. A., Sciare, J., Schlager, H., Schultz, M., Siegmund, P., Steil, B., Stephanou, E. G., Stier, P., Traub, M., Warneke, C., Williams, J., and Ziereis, H.: Global air pollution crossroads over the Mediterranean, Science, 298, 794-799, doi:10.1126/science.1075457, 2002.

Lensky, I. M., and Dayan, U.: Continuous detection and characterization of the Sea Breeze in clear sky conditions using Meteosat Second Generation, Atmos. Chem. Phys., 12, 6505-6513, doi :10.5194/acp-12-6505-2012, 2012.

Lensky, I. M., and Dayan, U.: Satellite observations of land surface temperature patterns induced by synoptic circulation, Int. J. Climatol., 35, 189–195. doi:10.1002/joc.3971, 2015.

Leventidou, E., Zanis, P., Balis, D., Giannakaki, E., Pytharoulis, I., and Amiridis, V.: Factors affecting the comparisons of planetary boundary layer height retrievals from CALIPSO,

ECMWF and radiosondes over Thessaloniki, Greece, Atmos. Environ., 74, 360-366, doi: 10.1016/j.atmosenv.2013.04.007, 2013.

Lieman, R., and Alpert, P.: Investigation of the planetary boundary layer height variations over complex terrain, Boundary-Layer Meteorol., 62, 129-142, doi:10.1007/BF00705550, 1993.

Liu, J. J., Jones, D. B. A., Worden, J. R., Noone, D., Parrington, M., and Kar, J.: Analysis of the summertime buildup of tropospheric ozone abundances over the Middle East and NorthAfrica as observed by the tropospheric emission spectrometer instrument, J. Geophys. Res., 114, D05304, doi :10.1029/2008JD010993, 2009.

Luria, M., Almog, H., and Peleg, M.: Transport and transformation of air pollutants from Israel's coastal area, Atmos. Environ., 18, 2215-2221, doi:10.1016/0004-6981(84)90209-9, 1984.

Luria, M., Peleg, M., Sharf, G., Siman Tov- Alper, D., Spitz, N., Ben Ami, Y., Gawii, Z., Lifschitz, B., Yitzchaki, A., and Seter, I.: Atmospheric sulfur over the east Mediterranean region, J. Geophys. Res., 101, 25917-25930, doi:10.1029/96JD01579, 1996.

Marmer, E., and Langmann, B.: Impact of ship emissions on the Mediterranean summertime pollution and climate: A regional model study, Atmos. Environ., 39, 26, 4659–4669, doi: 10.1016/j.atmosenv.2005.04.014, 2005.

Marmer, E., Dentener, F., Aardenne, J. V., Cavalli, F., Vignati, E., Velchev, K., Hjorth, J., Boersma, F., Vinken, G., Mihalopoulos, N., and Raes, F.: What can we learn about ship emission inventories from measurements of air pollutants over the Mediterranean Sea?, Atmos. Chem. Phys., 9, 6815–6831, doi:10.5194/acp-9-6815-2009, 2009.

Matvev, V., Dayan, U., Tass, I., and Peleg, M.: Atmospheric sulfur flux rates to and from Israel, Sci. Total Environ., 291, 143-154, doi:10.1016/S0048-9697(01)01089-0, 2002.

McElroy, J. L., and Smith, T. B.: Lidar description of mixing-layer thickness characteristics in a complex terrain/coastal environment, J. Appl. Meteor., 30, 585–597, doi:10.1175/1520-0450(1991)030<0585: LDOMLT>2.0.CO;2, 1991.

Meagher, J. F., Stockburger, L., Bonanno, R. J., Bailey, E. M., and Luria, M.: Atmospheric oxidation of flue-gases from coal-fired power-plants-A comparison between conventional and scrubbed plumes, Atmos. Environ., 15, 749–762, doi:10.1016/0004-6981(81)90279-1, 1981.

Michou, M., Saint-Martin, D., Teyssèdre, H., Alias, A., Karcher, F., Olivié, D., Voldoire, A., Peuch, V.-H., Clark, H., Lee, J.N. and Chéroux, F.: A new version of the CNRM Chemistry-Climate Model, CNRMCCM: description and improvements from the CCMVal2 simulations, Geosci. Model Dev., 4, 873-900, 2011, www.geosci-model-dev.net/4/1/2011, doi:10.5194/gmd-4-873-2011, 2011.

Mihalopoulos, N., Kerminen, V. M., Kanakidou, M., Berresheim, H., and Sciare, J.: Formation of particulate sulfur species (sulfate and methanesulfonate) during summer over the Eastern Mediterranean: A modelling approach, Atmos. Environ., 41, 6860–6871, doi: 10.1016/j.atmosenv.2007.04.039, 2007.

Moulin C., Lambert, C. E., Dayan, U., Masson, V., Ramonet, M., Bousquet, P., Legrand, M., Balkanski, Y. J., Guelle, W., Marticorena, B., Bergametti, G., and Dulac, F.: Satellite climatology of African dust transport in the Mediterranean atmosphere, J. Geophys. Res., 103, 13137-13144, doi:10.1029/98JD00171, 1998.

Myriokefalitakis, S., Daskalakis, N., Fanourgakis, G. S., Voulgarakis, A., Krol, M. C., Aan de Brugh, J. M. J., and Kanakidou, M.: Ozone and carbon monoxide budgets over the Eastern Mediterranean, Sci. Total Environ., 563–564, 40–52, doi: 10.1016/j.scitotenv.2016.04.061, 2016.

Nabat, P., Somot, S., Mallet, M., Chiapello, I., Morcrette, J. J., Solmon, F., Szopa, S., Dulac, F., Collins, W., Ghan, S., Horowitz, L. W., Lamarque, J. F., Lee, Y. H., Naik, V., Nagashima, T., Shindell, D., and Skeie, R.: A 4-D climatology (1979–2009) of the monthly tropospheric aerosol optical depth distribution over the Mediterranean region from a comparative evaluation and blending of remote sensing and model products, Atmos. Meas. Tech., 6, 1287-1314, doi:10.5194/amt-6-1287-2013, 2013.

Neumann, J.: Diurnal variation of the subsidence inversion and radio wave propagation phenomena over the coastal area of Israel, Israel Meteorological Service, Jerusalem, Series A, Meteorol. Notes, 16, 12 pp., 1952.

Nirel, R., and Dayan, U.: On the ratio of sulfur dioxide to nitrogen oxides as an indicator of air pollution sources, J. Appl. Meteorol., 40, 1209-1222, doi:10.1175/1520-0450(2001)040<1209: OTROSD>2.0.CO;2, 2001.

Novelli, P. C., Steele, L. P., and Tans, P. P.: Mixing ratios of carbon-monoxide in the troposphere, J. Geophys. Res.-Atmos., 97, 20731-20750, doi:10.1029/92JD02010, 1992.

Peleg, M., Luria, M., Setter, I., Perner, D., and Russel, P.: Ozone levels in central Israel, Isr. J. Chem., 34, 375–386, doi:10.1002/ijch.199400041, 1994.

Ranmar, D. O., Matveev, V., Dayan, U., Peleg, M., Kaplan, J., Gertler, A. W., Luria, M., Kallos, G., Katsafados, P., and Mahrer, Y.: The impact of coastal transportation emission of NOx and VOC on inland air pollution over Israel- Utilizing numerical simulations, airborne measurements and synoptic analysis, J. Geophys. Res., 107, 4331, doi:2001JD000808, 2002.

Ricaud, P., Sič, B., El Amraoui, L., Attié, J. -L., Zbinden, R., Huszar, P., Szopa, S., Parmentier, J., Jaidan, N., Michou, M., Abida, R., Carminati, F., Hauglustaine, D., August, T., Warner, J., Imasu, R., Saitoh, N., and Peuch, V. -H.: Impact of the Asian monsoon anticyclone on the variability of mid-to-upper tropospheric methane above the Mediterranean Basin, Atmos. Chem. Phys., 14, 11427-11446, doi:10.5194/acp-14-11427-2014, 2014.

Rindsberger, M.: Analysis of mixing depth over Tel-Aviv, Israel, J. Earth Sci., 23, 13-17, 1974.

Rindsberger, M.: Air pollution potential in greater Tel-Aviv area, Israel, J. Earth Sci., 25, 127-132, 1976.

Rodwell, M. J., and Hoskins, B. J.: Monsoons and the dynamics of deserts, Q.J.R. Meteorol. Soc., 122, 1385–1404, doi:10.1002/qj.49712253408, 1996.

Roelofs, G. J., Scheeren, H. A., Heland, J., Ziereis, H., and Lelieveld, J.: A model study of ozone in the Eastern Mediterranean free troposphere during MINOS (August 2001), Atmos. Chem. Phys., 3, 1199–1210, doi:10.5194/acp-3-1199-2003, 2003.

Rudich, Y., Kaufman, J., Dayan, U., Hongbin Y., and Kleidman, R. G.: Estimation of transboundary transport of pollution aerosols by remote sensing in the eastern Mediterranean, J. Geophys. Res – Atmos., 113, D14S13, doi:10.1029/2007JD009601, 2008.

Safieddine, S., Boynard, A., Coheur, P. -F., Hurtmans, D., Pfister, G., Quennehen, B., Thomas, J. L., Raut, J. -C., Law, K. S., Klimont, Z., Hadji-Lazaro, J., George, M., and Clerbaux, C.: Summertime tropospheric ozone assessment over the Mediterranean region using the thermal infrared IASI/MetOp sounder and the WRF-Chem model, Atmos. Chem. Phys., 14, 10119–10131, doi:10.5194/acp-14-10119-2014, 2014.

Sciare, J., Bardouki, H., Moulin, C., and Mihalopoulos, N.: Aerosol sources and their contribution to the chemical composition of aerosols in the eastern Mediterranean Sea during summertime, Atmos. Chem. Phys., 3, 291–302, doi:10.5194/acp-3-291-2003, 2003.

Sciare, J., Oikonomou, K., Cachier, H., Mihalopoulos, N., Andreae, M. O., Maenhaut, W., Sarda-Esteve, M.: Aerosol mass closure and reconstruction of the light scattering coefficient over the eastern Mediterranean Sea during the MINOS campaign, Atmos. Chem. Phys., 5, 2253–2265, doi:10.5194/acp-5-2253-2005, 2005.

Schneising, O., Buchwitz, M., Burrows, J. P., Bovensmann, H., Bergamaschi, P., and Peters, W.: Three years of greenhouse gas column-averaged dry air mole fractions retrieved from satellite. Part 2: Methane, Atmos. Chem. Phys., 9, 443–465, doi:10.5194/acp-9-443-2009, 2009.

Seinfeld, J. H., Urban air pollution: state of the science, Science, 243, 745–752, doi:10.1126/science.243.4892.745, 1989.

Sprenger, M., and Wernli, H.: A northern hemispheric climatology of cross-tropopause exchange for the ERA15 time period (1979–1993), J. Geophys. Res., 108, 8521, doi:10.1029/2002JD002636, 2003.

Stohl, A., James, P., Forster, C., Spinchtinger, N., Marenco, A., Thouret, V., and Smit, H. G. J.: An extension of MOZAIC ozone climatologies using trajectory statistics, J. Geophys. Res., 106, 27757–27768, doi:10.1029/2001JD000749, 2001.

Stunder, M., and Sethuraman, S.: A comparative evaluation of the coastal internal boundary layer height, Bound. -Layer Meteorol., 32, 177–204, doi:10.1007/BF00120934, 1985.

Teyssèdre, H., Michou, M., Clark, H. L., Josse, B., Karcher, F., Olivie, D., Peuch, V. -H., Saint-Martin, D., Cariolle, D., Attie, J. -L., Nedelec, P., Ricaud, P., Thouret, V., Van Der A, R. J., Volz-Thomas, A., and Cheroux, F., A new tropospheric and stratospheric Chemistry and Transport Model MOCAGE-Climat for multi-year studies: evaluation of the present-day climatology and sensitivity to surface processes. Atmos. Chem. Phys., 7, 5815-5860, <hal-00328553>

Tyrlis, E., and Lelieveld, J.: Climatology and dynamics of the summer Etesian winds over the Eastern Mediterranean, J. Atmos. Sci., 70, 3374–3396, doi:10.1175/JAS-D-13-035, 2013.

Večeřa, Z., Mikuška, P., Smolík, J., Eleftheriadis, K., Bryant, C., Colbeck, I., and Lazaridis, M.: Shipboard measurements of nitrogen dioxide, nitrous acid, nitric acid and ozone in the eastern Mediterranean Sea, Water Air Soil Poll., Focus 8, 117-125, doi:10.1007/s11267-007-9133-y, 2008.

Vinken, G. C. M., Boersma, K. F., van Donkelaar, A., and Zhang, L.: Constraints on ship NOx emissions in Europe using GEOS-Chem and OMI satellite NO2 observations, Atmos. Chem. Phys., 14, 1353–1369, doi:10.5194/acp-14-1353-2014, 2014.

Voulgarakis, A., Savage, N. H., Braesicke, P., Wild, O., Carver, G. D., and Pyle, J. A.: Interannual variability of tropospheric composition: The influence of changes in emission, meteorology and clouds, Atmos. Chem. Phys., 10, 2491-2506, doi:10.5194/acp-10-2491-2010, 2010.

Wanger, A., Peleg, M., Sharf, G., Mahrer, Y., Dayan, U., Kallos, G., Kotroni, V., Lagouvardos, K., Varinou, M., Papadopoulos, A., and Luria, M.: Some observational and modelling evidence of long-range transport of air pollutants from Europe towards the Israeli coast, J. Geophys. Res., 105, D6, 7177-7186, doi:10.1029/1999JD901060, 2000.

Yarnal, B.: Synoptic Climatology in Environmental Analysis, Belhaven Press, London, 1993.

Zanis, P., Hadjinicolaou, P., Pozzer, A., Tyrlis, E., Dafka, S., Mihalopoulos, N., and Lelieveld, J.: Summertime free-tropospheric ozone pool over the eastern Mediterranean/Middle East, Atmos. Chem. Phys., 14, 115–132, doi:10.5194/acp-14-115-2014, 2014.

Zbinden, R. M., Thouret, V., Ricaud, P., Carminati, F., Cammas, J. -P., and Nédélec, P.: Climatology of pure tropospheric profiles and column contents of ozone and carbon monoxide using MOZAIC in the mid-northern latitudes (24° N to 50° N) from 1994 to 2009, Atmos. Chem. Phys., 13, 12363-12388, doi:10.5194/acp-13-12363-2013, 2013.

Zbinden R. M., Ricaud, P., Catoire, V., Brocchi, V., Massart, S., El Amraoui, L., Attie, J. L., Nabat, P., Dulac, F., Hamonou, E., Dayan, U., Piguet, B., and the SAFIRE team: Processes affecting the tropospheric chemical variability over the Mediterranean Basin: results from the summer GLAM campaign, Atmospheric Processes in the Mediterranean (APM 2016): A joint ACTRIS - BACCHUS – CHArMEx Int. Workshop, 17-21 Oct. 2016, http://www.cyi.ac.cy/index.php/apm-workshop-2016-home.html., 2016.

Zhang, J. S., and Rao, S. T.: The role of vertical mixing in the temporal evolution of ground-level ozone concentrations, J. Appl. Meteor., 38, 1674–1691, doi:10.1175/1520-0450(1999)038<1674: TROVMI>2.0.CO;2, 1999.

Ziemke, J. R., Chandra, S., Labow, G. J., Bhartia, P. K., Froidevaux, L., and Witte, J. C.: A global climatology of tropospheric and stratospheric ozone derived from Aura OMI and MLS measurements, Atmos. Chem. Phys., 11, 9237–9251, doi:10.5194/acp-11-9237-2011, 2011.

Ziv, B., Saaroni, H., and Alpert, P.: The factors governing the summer regime of the eastern Mediterranean, Int. J. Climatol., 24, 1859-1871, doi:10.1002/joc.1113, 2004.

Atmos. Chem. Phys. Discuss., doi:10.5194/acp-2017-79, 2017
Manuscript under review for journal Atmos. Chem. Phys.
Discussion started: 30 March 2017

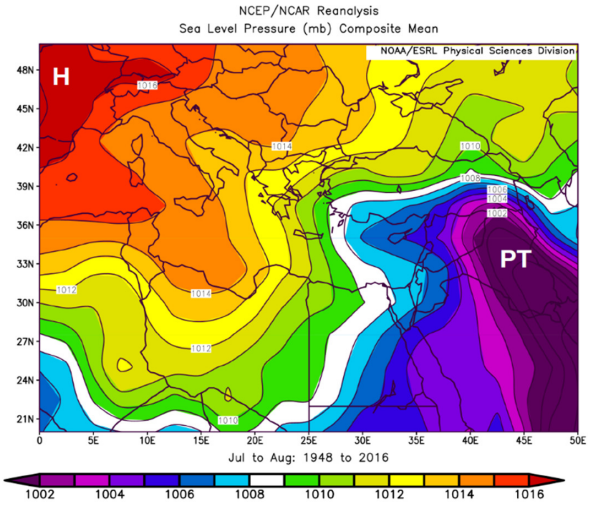

Figure 1. Composite long term mean Sea Level Pressure (hPa) for July-August over 1948-2016. "PT" indicates the Persian Trough position. "H" indicates the Anticyclone position. Source: NCEP Reanalysis data provided by the NOAA/OAR/ESRL PSD, Boulder, Colorado, USA, http://www.esrl.noaa.gov/psd/

Atmos. Chem. Phys. Discuss., doi:10.5194/acp-2017-79, 2017
Manuscript under review for journal Atmos. Chem. Phys.
Discussion started: 30 March 2017

Atmospheric Chemistry and Physics Discussions

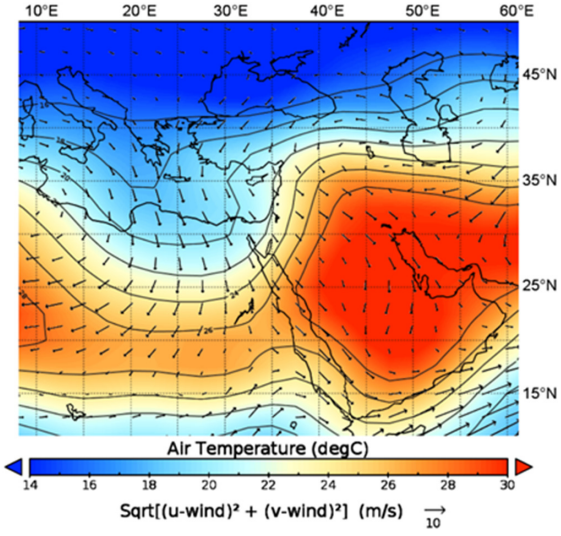

Figure 2. NCEP/NCAR reanalysis composite long-term mean temperature at 850 hPa (~1500 m, above sea level or a.s.l.) with wind vectors, averaged over 1948-2016 for July-August. Note the southward penetration of the European cold air over the Mediterranean Basin. This cold air mass is transported at shallow tropospheric layers towards the EM by the Etesian north-westerlies characterizing the Persian trough. Source: NCEP Reanalysis data provided by the NOAA/OAR/ESRL PSD, Boulder, Colorado, USA, http://www.esrl.noaa.gov/psd/.

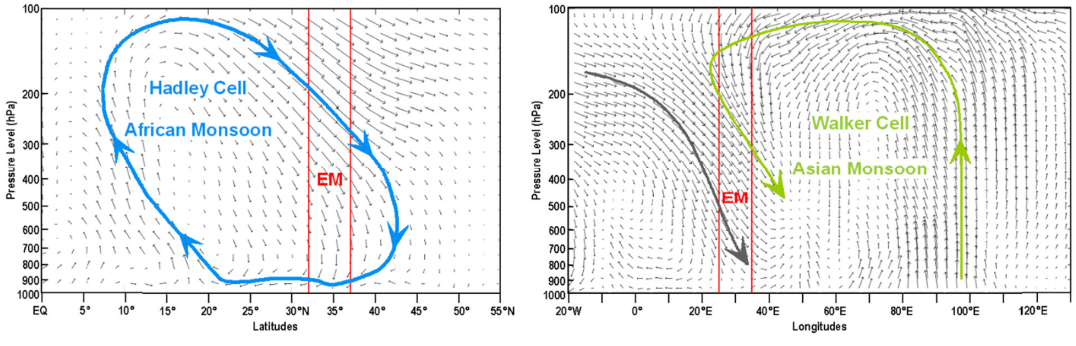

Figure 3. (Left) Closed Hadley cell circulation of the African Monsoon depicted by the vertical cross section of wind vectors for July-August averaged over the 30-40°E longitudinal band. (Right) Closed Walker cell circulation of the Asian Monsoon depicted by the vertical cross section of wind

Atmos. Chem. Phys. Discuss., doi:10.5194/acp-2017-79, 2017
Manuscript under review for journal Atmos. Chem. Phys.
Discussion started: 30 March 2017

Atmospheric Chemistry and Physics Discussions

vectors for July-August averaged over the 20-35°N latitudinal band. The two figures are based on the NCEP/NCAR long-term averages (1948-2016) with the position of the Eastern Mediterranean (EM) in red. Source: NCEP Reanalysis data provided by the NOAA/OAR/ESRL PSD, Boulder, Colorado, USA, http://www.esrl.noaa.gov/psd/.

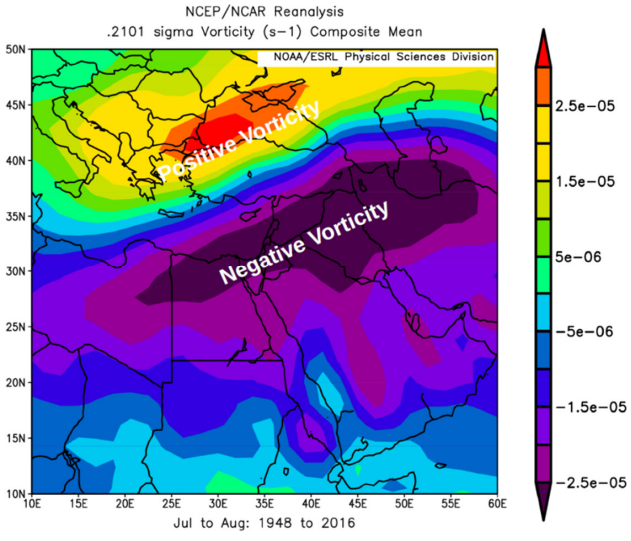

Figure 4. NCEP/NCAR Reanalysis long-term averages (1948-2016) of the relative vorticity at 200 hPa (~12 km a.s.l.) for July-August. The relative vorticity vector is generally perpendicular to the ground, positive when the vector points upward, negative when it points downward. Note the negative relative vorticity region located over the southeastern Mediterranean as a result from both shear and curvature negative relative vorticity. Relative vorticity units are 10^{-5} s^{-1}. Source: NCEP Reanalysis data provided by the NOAA/OAR/ESRL PSD, Boulder, Colorado, USA, http://www.esrl.noaa.gov/psd/.

Atmos. Chem. Phys. Discuss., doi:10.5194/acp-2017-79, 2017
Manuscript under review for journal Atmos. Chem. Phys.
Discussion started: 30 March 2017

Atmospheric Chemistry and Physics Discussions

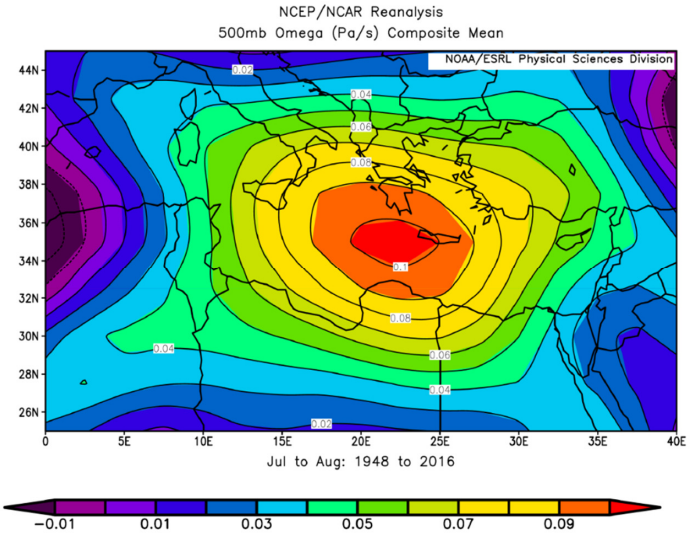

Figure 5. NCEP/NCAR reanalysis long-term averages of Omega (Pa s^{-1}) at 500 hPa (~5.5 km a.s.l.) designating vertical motion for July to August 1948-2016. The maximum subsidence of 0.1 Pa s^{-1} is equivalent to a downward air motion of ~1.5 cm s^{-1}. Source: NCEP Reanalysis data provided by the NOAA/OAR/ESRL PSD, Boulder, Colorado, USA, http://www.esrl.noaa.gov/psd/.

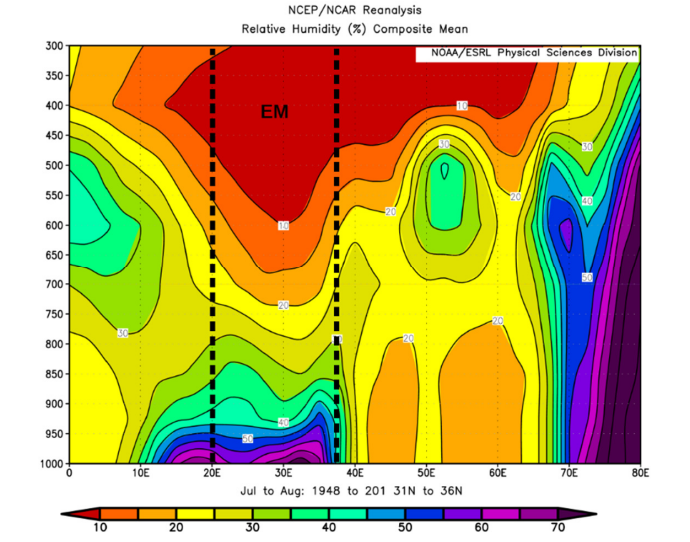

Atmos. Chem. Phys. Discuss., doi:10.5194/acp-2017-79, 2017
Manuscript under review for journal Atmos. Chem. Phys.
Discussion started: 30 March 2017

Atmospheric Chemistry and Physics Discussions

Figure 6. Long- term mean vertical cross section of relative humidity, averaged over the 31-36° N latitudinal band for July-August 1948-2016 with the Eastern Mediterranean position (EM), in dashed black lines. Source: NCEP Reanalysis data provided by the NOAA/OAR/ESRL PSD, Boulder, Colorado, USA, http://www.esrl.noaa.gov/psd/.

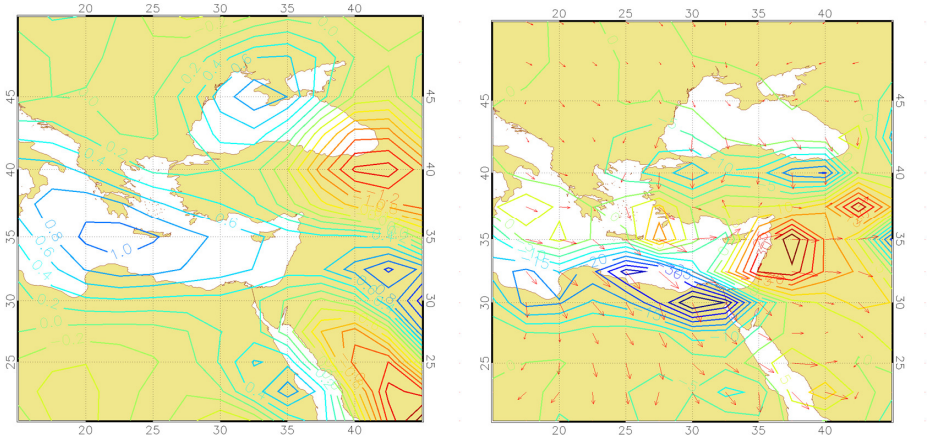

Figure 7. (Left) Blue contours display positive Omega values (cm s−1) representing the vertical descending air motion at a mid-tropospheric level (700 hPa) (~3 km a.s.l.) pointing at a core of 1 cm s−1 located over Crete. Red contours are negative Omega values. (Right) Blue contours display cold advection calculated as multiplication of the horizontal thermal gradient by the wind vector. Red contours indicate warm advection, both at 995 hPa level, equivalent to about 140 m a.s.l at 12:00 UTC during PT summer synoptic conditions. Source: NCEP Reanalysis data for 2000-2012, provided by the NOAA/OAR/ESRL PSD, Boulder, Colorado, USA, http://www.esrl.noaa.gov/psd/.

Atmos. Chem. Phys. Discuss., doi:10.5194/acp-2017-79, 2017
Manuscript under review for journal Atmos. Chem. Phys.
Discussion started: 30 March 2017

Atmospheric Chemistry and Physics Discussions

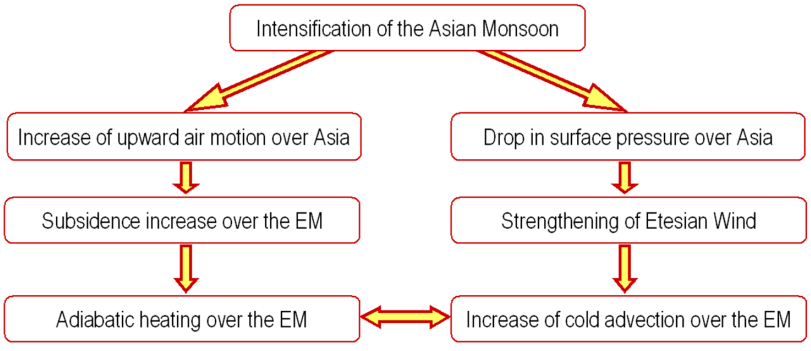

6

7 Figure 8. Schematic of the proposed mechanism during intensification of the Asian Monsoon
8 (adapted from Ziv et al., (2004), permission requested from John Wiley and Sons).

9

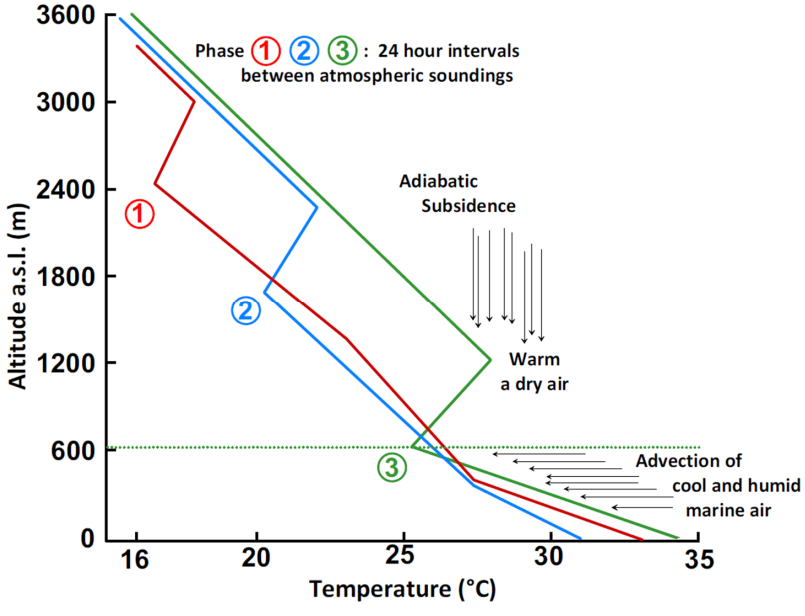

10

11 Figure 9. Successive schematic sounding thermal profiles indicating the downward motion of
12 adiabatic subsidence accompanied by a weakening of the Persian Trough which restricts the MLD
13 to shallow layer of the atmosphere (phases 1-3 are 24 h intervals between each sounding at Beit-
14 Dagan, Israel); (from Dayan et al. (1988), ©American Meteorological Society. Used with
15 permission).

Atmos. Chem. Phys. Discuss., doi:10.5194/acp-2017-79, 2017
Manuscript under review for journal Atmos. Chem. Phys.
Discussion started: 30 March 2017

Atmospheric Chemistry and Physics Discussions

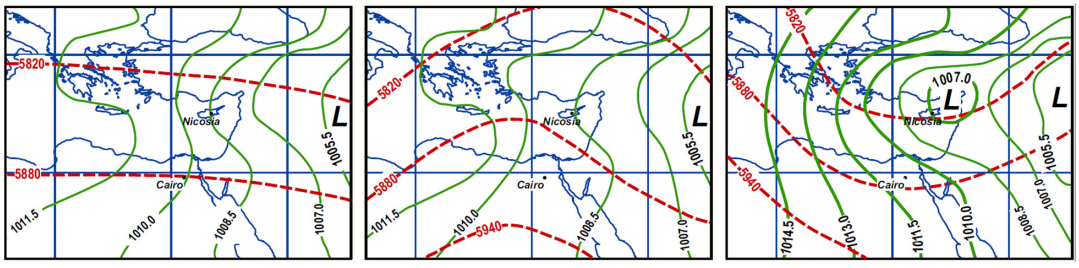

Figure 10. Typical synoptic charts showing the three modes: (a) moderate, (b) shallow, and (c) deep mode of the Persian Trough as defined by the surface-pressure differences between Nicosia (Cyprus) and Cairo (Egypt), and their associated upper level conditions. Solid lines are isobars of sea level pressure with 1.5-hPa intervals. Dashed lines are contours at 500-hPa level with 60-m intervals (from Dayan et al. (2002), ©American Meteorological Society. Used with permission).

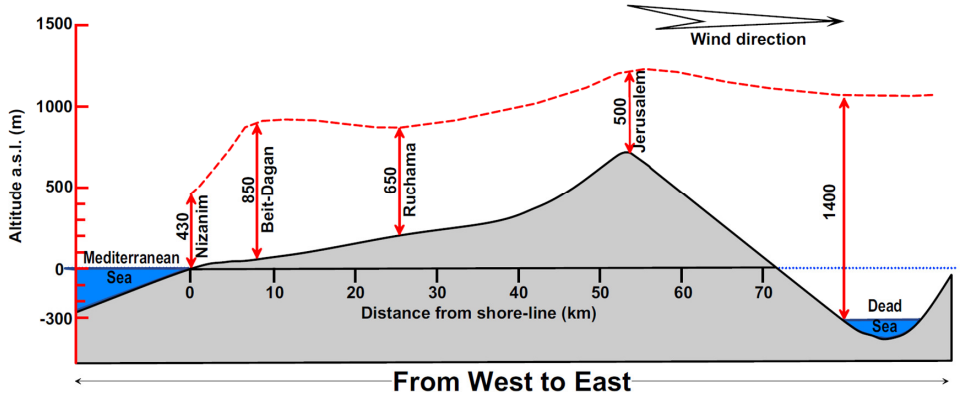

Figure 11. Schematic description of the lateral variation of the mixing layer depth from the Mediterranean Sea to the Dead Sea (from Dayan et al. (1988), ©American Meteorological Society. Used with permission).

Atmos. Chem. Phys. Discuss., doi:10.5194/acp-2017-79, 2017
Manuscript under review for journal Atmos. Chem. Phys.
Discussion started: 30 March 2017

Atmospheric Chemistry and Physics Discussions

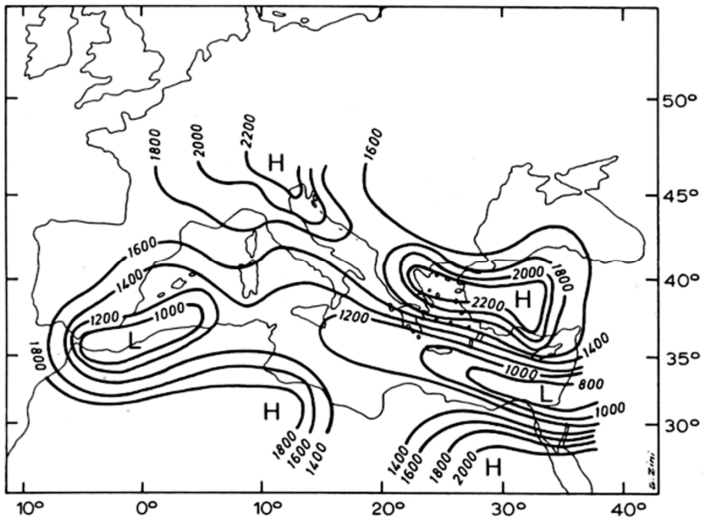

Figure 12. Seasonal map of the mixing layer depth (MLD, in m) for summer (JJA) 1987 over the Mediterranean region at 12:00 UTC (from Dayan et al. (1996), permission requested from Kluwer Academic Publishers).

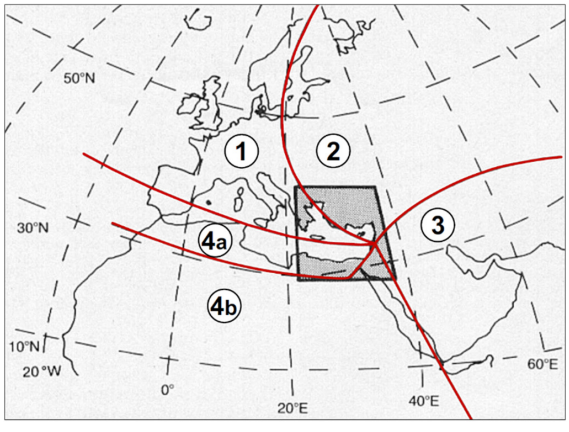

Figure 13. Trajectory typing method used to categorize 5-day back-trajectories from the EM region at 850 hPa using the Air Resources Laboratory's trajectory model GAMBIT over the 1978-1982 period (from Dayan (1986), ©American Meteorological Society. Used with permission).

Atmos. Chem. Phys. Discuss., doi:10.5194/acp-2017-79, 2017
Manuscript under review for journal Atmos. Chem. Phys.
Discussion started: 30 March 2017

Atmospheric Chemistry and Physics Discussions

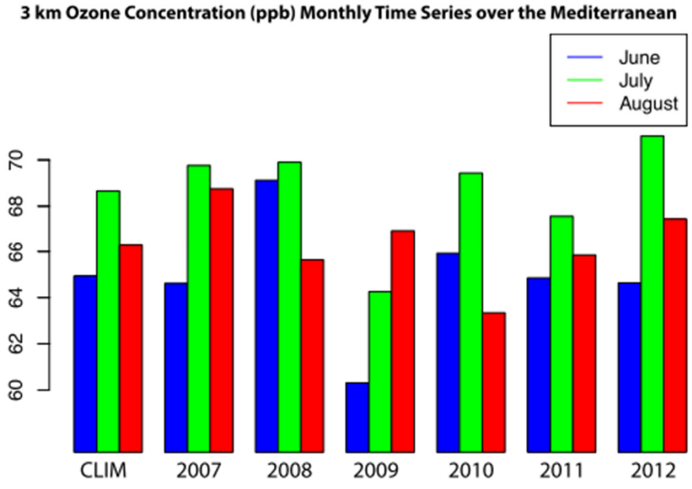

Figure 14. Monthly means of O_3 concentrations (ppbv) at 3 km partial column measured by IASI in summer (JJA) within the 2007-2012 period over the Mediterranean (IASI morning overpasses). Only the observations over the sea are considered in the averages. The monthly means referred to as "CLIM" represent the averages over the whole period (reproduced from Doche et al., 2014).

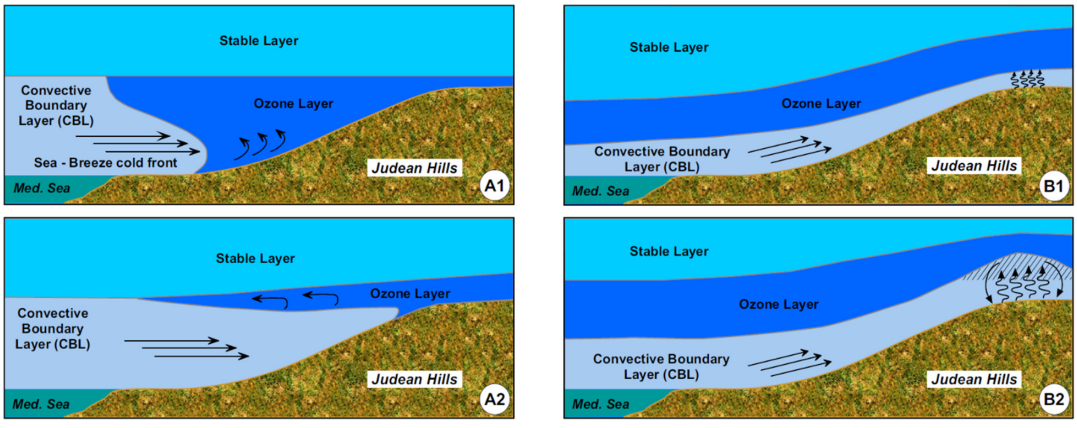

Figure 15. Scheme of the mechanism causing fumigation of a rich O_3 cloud toward the ground as moving inland over the EM coast during the weakening of a deep mode of the PT (from Dayan and Koch (1996), ©American Meteorological Society. Used with permission).

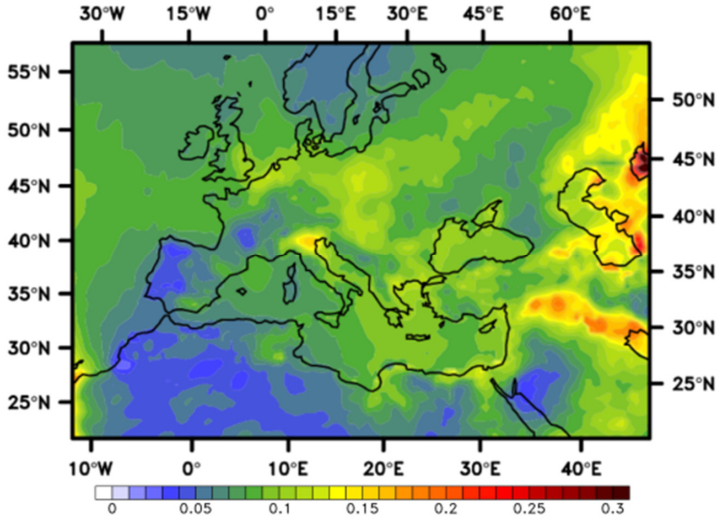

Fig. 16: Average aerosol optical depth contributed by particulate sulfate validated against AERONET AOD observations over the period 2003–2009. As mentioned by http://www.esrl.noaa.gov/gmd/grad/surfrad/aod/ , a value of 0.01 corresponds to an extremely clean atmosphere, and a value of 0.4 to a very hazy condition (The 2003-2010 average AOD over the Mediterranean Basin is ~0.20 (reproduced from Nabat et al., 2013)

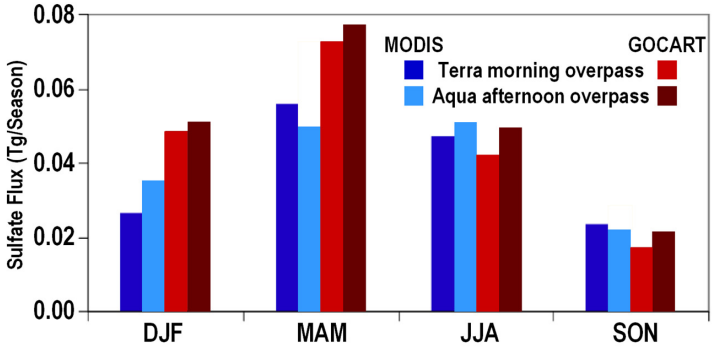

Figure 17. Comparison of MODIS space-borne and GOCART model derived estimates of the seasonal flux (Tg season^{-1}) of dry sulfate to the EM along the 150-km Israeli coastline. (a) MODIS/Terra overpass and (b) MODIS/Aqua overpass (adapted from Rudich et al., 2008).

Atmos. Chem. Phys. Discuss., doi:10.5194/acp-2017-79, 2017
Manuscript under review for journal Atmos. Chem. Phys.
Discussion started: 30 March 2017

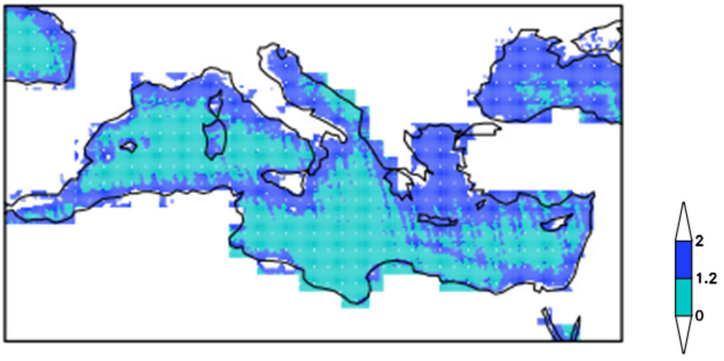

Figure 18. Seasonal average over June-August 2006 of NO_2 columns over the Mediterranean Sea (1015 molecules cm^{-2}), retrieved from the OMI satellite and considering only maritime pixels (reproduced from Marmer et al., 2009).

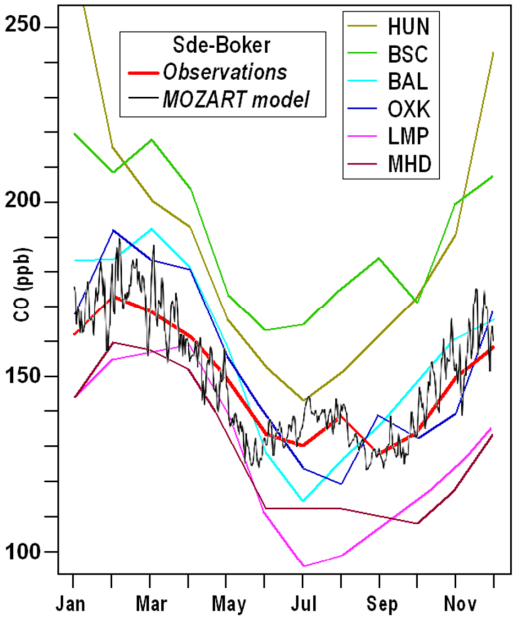

Figure 19. CO monthly mean concentrations over 1996-2009 at Sde-Boker (red) and at seven European ESRL/GMD background stations (defined in Table 3, multiple colors), compared to the

Atmos. Chem. Phys. Discuss., doi:10.5194/acp-2017-79, 2017
Manuscript under review for journal Atmos. Chem. Phys.
Discussion started: 30 March 2017

1 five-year averaged CO surface concentrations at Sde-Boker (black) over 2003-2007 from the
2 MOZART-4 chemistry-transport model (adapted from Drori et al., 2012).

3

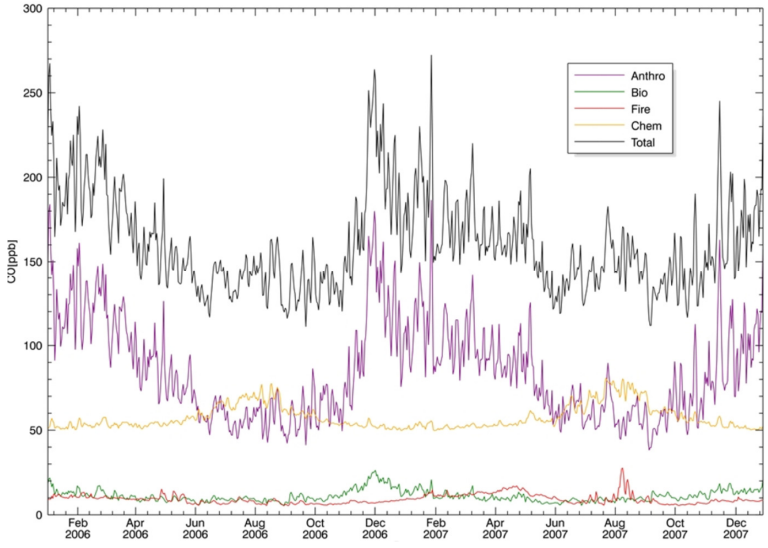

4

5 Figure 20. Total CO (black) over Sde-Boker as simulated by MOZART for 2006–2007 and
6 specific sources contributing to the CO surface: anthropogenic (purple), chemical production
7 (orange), biogenic (green) and fires (red) (adapted from Drori et al., 2012).

8

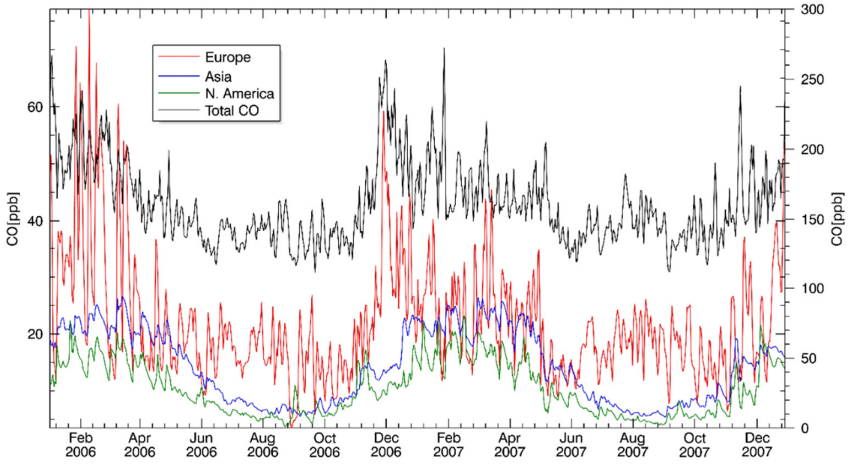

9

Atmos. Chem. Phys. Discuss., doi:10.5194/acp-2017-79, 2017
Manuscript under review for journal Atmos. Chem. Phys.
Discussion started: 30 March 2017

Figure 21. The European (red), Asian (blue) and North American (green) anthropogenic contribution to the total surface CO (black) at Sde-Boker as simulated by MOZART over 2006-2007. Distinct continents are scaled on the left vertical axis and total CO on the right vertical axis (adapted from Drori et al., 2012).

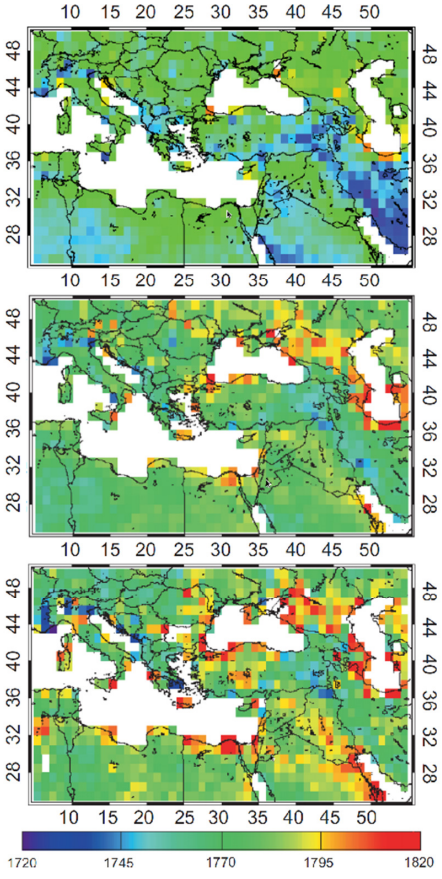

Figure 22. Maps by 1° × 1° resolution of SCIAMACHY WFM-DOAS XCH_4 levels in 2003 including a yearly average (top panel), a summer average (mid-panel) and an August average (bottom panel), in ppbv (from Georgoulias et al. (2011), permission requested from Taylor and Francis).

Atmos. Chem. Phys. Discuss., doi:10.5194/acp-2017-79, 2017
Manuscript under review for journal Atmos. Chem. Phys.
Discussion started: 30 March 2017

Atmospheric Chemistry and Physics Discussions

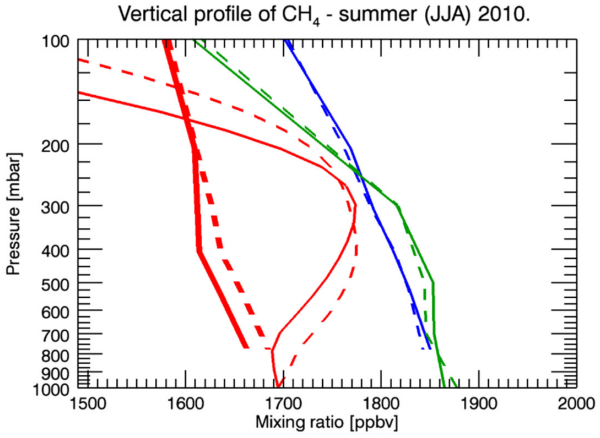

Fig. 23: Summer averaged vertical profiles of CH_4 as measured by AIRS (blue lines) and GOSAT (green lines), and as calculated by MOCAGE (thin red lines) over the Eastern (dashed lines) and Western (solid lines) Mediterranean Basins in summer 2010. Also shown are the seasonally-averaged MOCAGE profiles convolved with the AIRS averaging kernels (thick red lines) for the summer over the Eastern (dashed lines) and Western (solid lines) Mediterranean Basins (adapted from Ricaud et al., 2014).

Atmos. Chem. Phys. Discuss., doi:10.5194/acp-2017-79, 2017
Manuscript under review for journal Atmos. Chem. Phys.
Discussion started: 30 March 2017

Atmospheric Chemistry and Physics Discussions

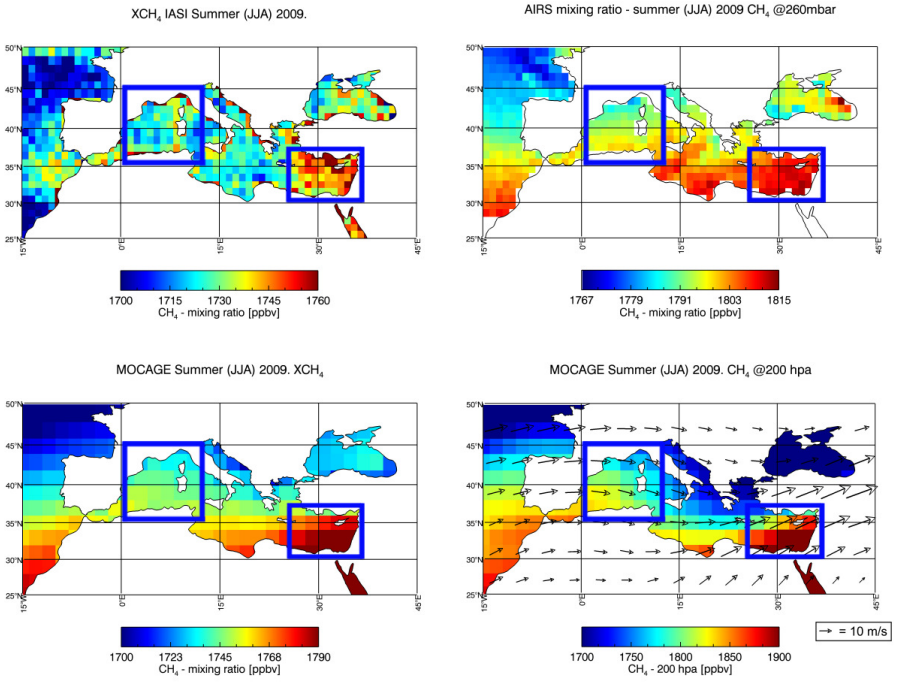

1

2 Figure 24: Fields of CH_4 as calculated by MOCAGE (bottom) and as measured by IASI (top left)
3 in total column and AIRS (top right) at 260 hPa averaged for summer JJA 2009. Horizontal winds
4 are from ARPEGE averaged over the same period. The two blue squares represent the West and
5 East Mediterranean Basins (adapted from Ricaud et al., 2014).

6

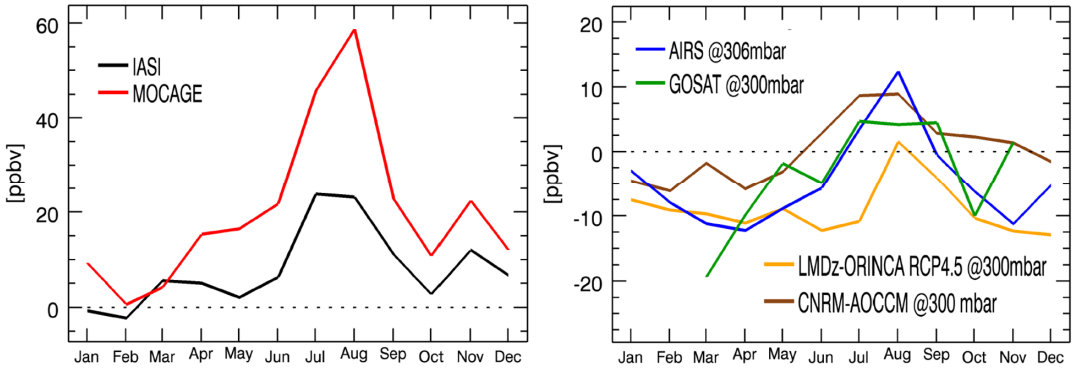

7

Figure 25: Seasonal evolution of the difference in CH_4 fields between the Eastern and Western MB: (right) around 300 hPa as measured by AIRS (blue) and GOSAT (green) and as calculated by LMDz-OR-INCA (yellow) and CNRM-AOCCM (brown), and (left) in total column as measured by IASI and calculated by MOCAGE (adapted from Ricaud et al. 2014).

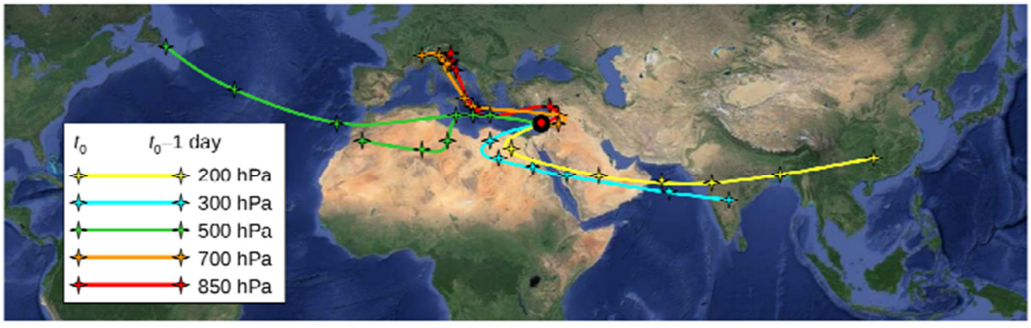

Figure 26: Six-day back-trajectories climatology from the point at 33°N and 35°E located in the Eastern Mediterranean Basin (red filled circle) derived for July-August over 2001-2010 every 12 hours. The position of the gravity center of each distribution (i.e. the maximum in the probability density function) at each level is represented every 24 h by a star. (adapted from Ricaud et al., 2014).

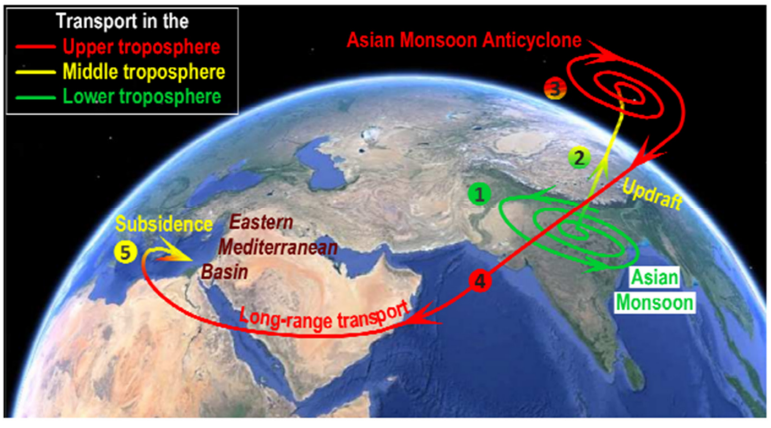

Atmos. Chem. Phys. Discuss., doi:10.5194/acp-2017-79, 2017
Manuscript under review for journal Atmos. Chem. Phys.
Discussion started: 30 March 2017

Atmospheric Chemistry and Physics Discussions

Figure 27: Schematic representation of the processes impacting the mid-to-upper tropospheric pollutants, including CH_4 above the EM in summer (July-August) (adapted from Ricaud et al., 2014).